JGR Biogeosciences

RESEARCH ARTICLE
10.1029/2025JG008970

Diapycnal Nutrient Fluxes and a Practical Assessment of the Biological Nutrient Trap in the North and South Atlantic Subtropical Gyres

S. C. Painter[1], **G. A. Tarran**[2], **A. P. Rees**[2], **and E. M. S. Woodward**[2]

[1]National Oceanography Centre, Southampton, UK, [2]Plymouth Marine Laboratory, Plymouth, UK

Key Points:

- Oceanic diapycnal nutrient fluxes are spatially variable but are lowest in subtropical latitudes
- Picoeukaryote nitrate uptake is sufficient to consume diapycnal nitrate fluxes isolating surface waters from deeper nutrient reservoirs
- Diapycnal nutrient fluxes may be only weakly relevant to global model predictions of how primary production may change in a warmer ocean

Supporting Information:

Supporting Information may be found in the online version of this article.

Correspondence to:

S. C. Painter,
stuart.painter@noc.ac.uk

Citation:

Painter, S. C., Tarran, G. A., Rees, A. P., & Woodward, E. M. S. (2025). Diapycnal nutrient fluxes and a practical assessment of the biological nutrient trap in the North and South Atlantic subtropical gyres. *Journal of Geophysical Research: Biogeosciences*, *130*, e2025JG008970. https://doi.org/10.1029/2025JG008970

Received 27 MAR 2025
Accepted 16 NOV 2025

Author Contributions:

Conceptualization: S. C. Painter
Data curation: S. C. Painter, G. A. Tarran, E. M. S. Woodward
Formal analysis: S. C. Painter
Funding acquisition: A. P. Rees
Investigation: S. C. Painter
Visualization: S. C. Painter
Writing – original draft: S. C. Painter
Writing – review & editing: S. C. Painter, G. A. Tarran, A. P. Rees, E. M. S. Woodward

Abstract Diapycnal mixing supplies nutrients to the euphotic zone, which in oligotrophic regions may substantially support rates of new production. However, the consensus view that diapycnal nutrient fluxes support new production within the *entire* euphotic zone is challenged by deep living autotrophs that likely consume some, if not all, of the diapycnal flux at depth. Quantifying how much of the diapycnal nitrate flux is trapped by biological consumption immediately above the nitracline remains challenging and the implications of nutrient trapping for comparisons of cross-nitracline diapycnal fluxes with euphotic zone integrals of new production remains unclear. It is increasingly important therefore to determine *where* in the euphotic zone the diapycnal flux has impact. In this study, a simple assessment is presented of the strength of the "nutrient trap," which is attributed to picoeukaryotes, a widely distributed group of autotrophic picoplankton found in the subtropical and tropical ocean. This study finds significant potential for the total consumption of diapycnal nutrient fluxes within a few meters of the nitracline, thus largely negating the significance of vertical diffusive fluxes for processes occurring at shallower depths. These results suggest that the significance of diapycnal nutrient fluxes for integrated productivity estimates is lower than generally assumed. Yet, although diapycnal fluxes cannot be entirely discounted from nutrient budgets due to seasonality in the consumption of such fluxes at depth, this likely makes harder current modeling efforts to constrain future ocean productivity where predictions of increased stratification generally favor greater reliance upon the diapycnal pathway to support production.

Plain Language Summary The study of nutrient supply pathways to surface waters of the remote tropical and subtropical ocean assumes a background contribution from diffusion, though the magnitude and variability of this process remains insufficiently quantified. Some studies argue that weak vertical nutrient gradients preclude diffusivity as a contributor to upper ocean nutrient pools leading to questions over where in the surface ocean diffusive nutrient supplies have their greatest impact. Here, we demonstrate that this speculative assumption may be correct and that picoeukaryotes, a widely distributed group of photosynthetic organisms known to favor conditions of low light and moderate nitrate concentrations are capable of consuming ("trapping") diffusive nutrient fluxes at depth isolating surface waters from deeper ocean nutrient reservoirs. That picoeukaryotes emerge as having a controlling influence on diffusive nutrient fluxes to overlying waters and at times completely consuming them is significant because numerical model-based predictions of future ocean productivity suggest increased reliance upon diffusion as other nutrient supply pathways are weakened by increased stratification in a warmer world. However, higher temperatures also increase metabolic processes and may influence picoeukaryote nutrient demand further impacting deeper nutrient gradients, picoeukaryote demand for nitrate, diffusive flux magnitudes, and ultimately productivity trends in subtropical waters.

1. Introduction

The diapycnal flux of nutrients across the oceanic nutricline into the euphotic zone is often considered to be a continuous nutrient supply pathway supporting new production yet the magnitude and variability of this supply term is still poorly known (Fernandez-Castro et al., 2014; Mouriño-Carballido et al., 2021). Under steady-state assumptions, and within experimental errors, diapycnal nitrate fluxes in low-latitude regions may balance phytoplankton nitrate demand across the euphotic zone (Lewis et al., 1986). Although the wider applicability of this broad equivalence for new production estimates has weakened with time particularly given the identification and significance of alternative nutrient supply pathways (nitrification (Clark et al., 2008, 2022; Yool et al., 2007), nitrogen fixation (Mahaffey et al., 2005; Moore et al., 2009), atmospheric deposition (Baker et al., 2003, 2006,

2007, 2013; Jickells et al., 2016)), more recent studies have instead emphasized that nitrate fluxes remain a critical factor controlling picoplankton community structure (Mouriño-Carballido et al., 2016; Otero-Ferrer et al., 2018; Villamaña et al., 2019).

Yet, it has still to be determined *where* in the euphotic zone diapycnal nutrient fluxes have their greatest impact and for the subtropical ocean whether comparison to nutrient uptake rates integrated across an oligotrophic water column is valid. Indeed, Karl (2010) noted that "*the near-zero nutrient concentration gradient observed in the upper 100 m of the water column suggests that continuous vertical nutrient flux cannot be the primary source of dissolved nutrients to the upper euphotic zone*." One interpretation of this statement is that diffusive fluxes are vertically limited in their impact. Separately, observations of a seasonal oscillation in the depth and gradient of the oceanic nitracline in response to changes in irradiance (Letelier et al., 2004) are suggestive of a controlling biological mechanism operating in the vicinity of the nitracline. This oscillation of the nitracline depth upwards toward the sea surface in winter and downwards away from the sea surface in summer with corresponding changes to the nitracline gradient (weaker in winter, stronger in summer) and coincident movement of the deep chlorophyll maximum (Karl et al., 2021) suggests a role for autotrophic organisms in the movement of the nitracline and thus in the consumption of nitrate at depth. Recently, Xing et al. (2023; and references therein) highlighted the dual roles of irradiance and nitracline depth in influencing the depth and picoplankton community diversity of the deep chlorophyll maximum, a ubiquitous feature of the subtropical ocean (Robinson et al., 2006), closely implying that there are ecologically significant feedbacks associated with the irradiance-driven seasonal movement of the nitracline and associated change to diapycnal nutrient fluxes that likely impact nutrient supply to the upper euphotic zone.

It follows therefore that changes to NO_3^- consumption must occur if the nitracline depth moves vertically and if the nitracline gradient changes. High resolution observations of NO_3^- uptake at the nitracline however remain limited but appear to show that rates exceed in situ productivity requirements implying that nitrogen and carbon assimilation are decoupled with the potential for a nitrate sink at the base of the euphotic zone (Painter et al., 2007) potentially driven by autotrophic picoeukaryotes (Painter et al., 2014). Picoeukaryotes are notable for displaying a deep abundance maximum in subtropical waters and can make significant contributions to the deep chlorophyll maximum (Zubkov, Sleigh, & Burkill, 2000; Zubkov, Sleigh, Burkill, & Leakey, 2000 Tarran et al., 2006). Picoeukaryotes (most likely heterotrophic) are also distributed widely throughout the deep ocean (Giner et al., 2020; Junger et al., 2023). As picoeukaryotes respond strongly to nitrate availability (Fernandez-Gonzalez et al., 2022), have high affinity for NO_3^- (Fawcett et al., 2011; Flombaum et al., 2020), and have previously been implicated in nitrate uptake deep in the euphotic zone (Painter et al., 2014), they are therefore a key group to consider when assessing whether deep-living phytoplanktons have the potential to trap or significantly modify diapycnal nutrient fluxes, thereby impacting productivity in the waters above. Previous studies have indicated that it is both feasible and highly likely that phytoplankton associated with the deep chlorophyll maximum consumes the cross-nitracline nitrate flux severing the link between deeper oceanic nutrient reservoirs and the upper euphotic zone (e.g., Anderson, 1969; Banse, 1987; Jamart et al., 1977). This premise, however, has never been satisfactorily investigated in an empirical sense and it remains unclear if the biological nutrient trap is an efficient and absolute sink for diapycnal nutrient fluxes, invalidating the diffusive flux as a critical source of nitrate to the upper euphotic zone (Karl, 2010), or whether the biological nutrient trap is inefficient or "leaky" allowing a proportion of the cross nitracline flux to potentially reach the upper ocean where it remains relevant for new production (Lewis et al., 1986).

The objectives of this study are to provide a simple proof of concept that biological regulation of diapycnal nutrient fluxes is significant and to also quantify the magnitude of the nutrient trap, which is suspected to be operating within the lower euphotic zone of the subtropical ocean by focusing upon the deep-living communities of picoeukaryotes present across the subtropical ocean.

2. Methods

2.1. Data Sources and Overview

Upper ocean (0–300 m) hydrographic profiles (temperature, salinity, and density), macronutrient measurements (total nitrate ($NO_3^- + NO_2^-$), nitrite (NO_2^-), phosphate (PO_4^{3-}) and silicate (SiO_4)), and flow cytometry observations of pico- and nanoplankton abundances collected during 18 cruises of the Atlantic Meridional Transect (AMT) program form the basis for this analysis (Table 1 and Tables S1–S3 in Supporting Information S1) (Aiken

Table 1
Summary of AMT Cruises Used in This Analysis Including Cruise Dates, Departure/Arrival Ports, Direction of Travel Northwards (N) or Southwards (S) Through the Atlantic Ocean and the Number of Sampled Stations

Cruise	Start date	End date	Departure	Arrival	Direction	No. Stns
AMT12	12/05/2003	17/06/2003	Port Stanley	UK	N	69
AMT13	10/09/2003	14/10/2003	UK	Port Stanley	S	76
AMT14	26/04/2004	02/06/2004	Port Stanley	UK	N	89
AMT15	17/09/2004	29/10/2004	UK	Cape Town	S	105
AMT16	19/05/2005	29/06/2005	Cape Town	UK	N	68
AMT17	15/10/2005	28/11/2005	UK	Cape Town	S	59
AMT18	03/10/2008	10/11/2008	UK	Port Stanley	S	100
AMT19	13/10/2009	01/12/2009	UK	Chile	S	119
AMT20	12/10/2010	15/11/2010	UK	Chile	S	88
AMT21	29/09/2011	14/11/2011	UK	Chile	S	73
AMT22	10/10/2012	24/11/2012	UK	Chile	S	74
AMT23	07/10/2013	08/11/2013	UK	Falklands	S	65
AMT24	21/09/2014	06/11/2014	UK	Chile	S	70
AMT25	11/09/2015	04/11/2015	UK	Falklands	S	73
AMT26	20/09/2016	04/11/2016	UK	Falklands	S	72
AMT27	21/09/2017	05/11/2017	UK	Falklands	S	79
AMT28	23/09/2018	30/10/2018	UK	Falklands	S	62
AMT29	13/10/2019	25/11/2019	UK	Chile	S	55

& Bale, 2000; Rees et al., 2015, 2024; Robinson et al., 2006, 2009). Since 1995, the AMT program has conducted repeated large-scale (>10,000 km long) surveys of the open waters of the Atlantic Ocean between the UK and destinations in the South Atlantic including South America, the Falkland Island and South Africa (Figure 1). We focus here on nutrient and picoplankton community data from AMT cruises 12–29, which cover the period 2003–2019, with earlier cruises (AMT1-11) omitted due to irregular sampling of the picoplankton community. A total of 1,121 nutrient profiles and up to 1,099 flow cytometry profiles (species dependent) were analyzed.

Nutrient concentrations were obtained from discrete water samples collected via CTD casts with between 12 and 24 depths sampled per cast providing a vertical sampling resolution of <5 to 20 m around the nitracline (cruise dependent). Samples were always analyzed on-board using a segmented flow colorimetric autoanalyzer. Methodologies typically followed Brewer and Riley (1965) for nitrate, Grasshoff (1976) for nitrite, and Kirkwood (1989) for phosphate and silicate except for nutrient data from AMT28, which used methodologies by Armstrong et al. (1967) for nitrate, nitrite, and silicate, and Bernhardt and Wilhelms (1967) for phosphate. Concentrations are reported in units of μmol L^{-1} in the source data files with typical detections limits of 0.02–0.05 μmol L^{-1} for total nitrate (nitrate + nitrite), 0.01–0.05 μmol L^{-1} for nitrite, 0.004–0.02 μmol L^{-1} for phosphate, and 0.05 μmol L^{-1} for silicate. High sensitivity nanomolar measurements for nitrate, nitrite, and phosphate were not included in this analysis as such data have not been collected routinely on all AMT cruises. The absence of such data does not influence the conclusions of this study as the focus is on the various nutriclines, which are adequately resolved via traditional analytical techniques.

The flow cytometry data sets for each cruise typically contained abundances (cells per ml^{-1}) of 6 phytoplankton groups identified as *Prochlorococcus*, *Synechococcus*, picoeukaryotes (<2 μm), cryptophytes, coccolithophores, and other nanoeukaryote phytoplankton (2–12 μm). Samples were collected via CTD cast with between 12 and 24 depths sampled across the upper 300 m of the water column. All samples were analyzed with consistent protocols using a Becton Dickson FACSort flow cytometer. Further analytical details are provided by Zubkov, Sleigh, and Burkill (2000), Zubkov, Sleigh, Burkill, and Leakey (2000), Zubkov et al. (1998), and Tarran et al. (2006). The number of usable abundance profiles varied by phytoplankton group and ranged from 849 (cryptophyes) to 1,099 (*Synechococcus*).

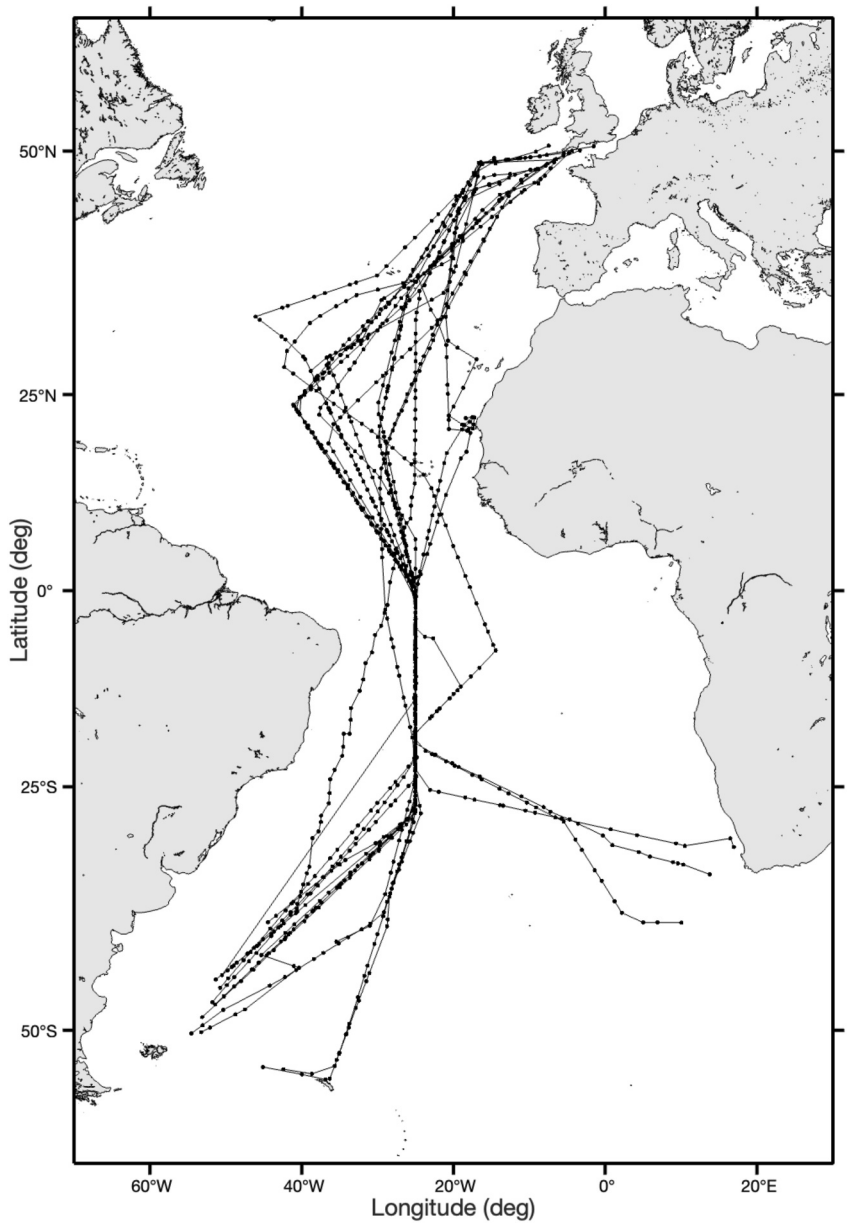

Figure 1. Cruise transects for Atlantic Meridional Transect cruises 12–29 (2003–2019).

2.2. Data Analysis

2.2.1. Data Handling

The individual cruise nutrient and flow cytometry cell count data sets were merged before being interpolated to a 1 m vertical grid to match the resolution of the hydrographic data. Interpolated profiles were used to calculate vertical gradients for all variables (nutrients and cell counts) based on the slope of depth versus concentration and using the central finite difference method before the maximum gradient and depth of the maximum gradient were identified within each profile. A visual examination of each profile was performed to ensure that nitrate concentrations and picoeukaryote abundances were correctly interpolated and that vertical gradients were robustly estimated.

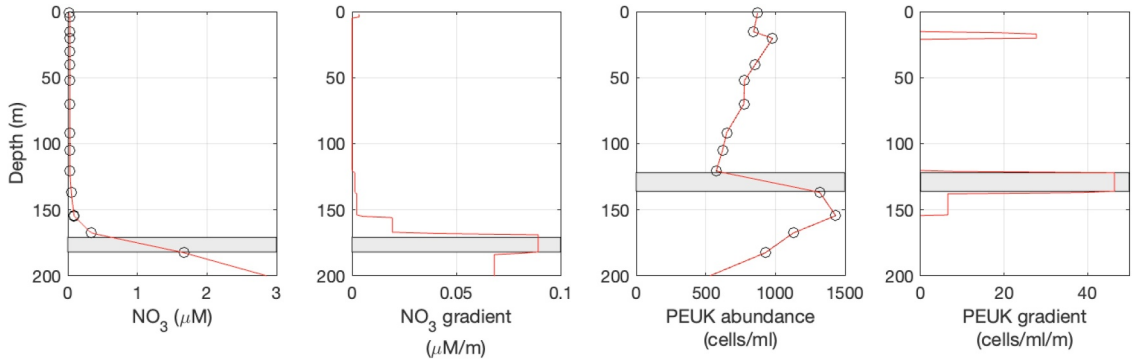

Figure 2. Example profile (AMT22 CTD051, 18.5298°W 25.1015°S). Gray shaded regions indicate where the maximum gradient in nitrate concentration and in picoeukaryote abundance were identified. Panel (a) the measured nutrient profile (black circles) and the interpolated nutrient profile (red line), (b) the vertical nutrient gradient profile, (c) the measured picoeukaryote (PEUK) cellular abundance (black circles) and the interpolated picoeukaryote cellular abundance (red line), and (d) the vertical picoeukaryote cellular abundance gradient profile.

2.2.2. Calculation of Vertical Gradients

2.2.2.1. Nutrients

The nitracline, phosphocline, and silicicline are defined here as the depth of the maximum vertical gradient in nitrate, phosphate, and silicate concentrations, respectively (Figure 2). This definition side-steps the subjective practice of using a predefined concentration (e.g., 100 nmol L^{-1} or 1 µmol L^{-1}) or analytical detection limit to define a particular nutricline, which can introduce ambiguities into definitions, artificial offsets between the major nutricline depths, inconsistencies between studies or forcibly define a feature using biologically inaccurate criteria. It is presumed that the various nutriclines can and do differ in depth as a result of differences in in situ nutrient demand, remineralization, and dissolution rates that is, P > N > Si (Hopkinson & Vallino, 2005; Hopkinson et al., 2002, 1997; Lonborg, 2009). Although the maximum gradient approach is arguably more biologically relevant than a fixed concentration approach, as it is related to the true vertical nutrient gradient that autotrophic organisms encounter (as opposed to a fixed nutrient concentration that may be above or below half-saturation constants or be above or below critical irradiance thresholds), the maximum gradient approach is not immune from subjectivity as the maximum gradient can be influenced by vertical sampling resolution and may be found over a range of (usually contiguous) depths rather than at one single depth. In such circumstances, an average depth for the maximum gradient was calculated.

2.2.2.2. Phytoplankton Groups

The six phytoplankton groups resolved by flow cytometry (*Prochlorococcus*, *Synechococcus*, picoeukaryotes, cryptophytes, coccolithophores, and other nanoeukaryote phytoplankton) have different distributions, abundances, and nutritional strategies. Under stratified and quiescent conditions, these phytoplankton groups, and even individual species, can exhibit clear vertical zoning with peak abundances located at different depths in the water column in response to local irradiance, nutrient availability, or other environmental conditions (Latasa et al., 2017; Poulton et al., 2017; Tarran et al., 2006; Zubkov, Sleigh, & Burkill, 2000; Zubkov, Sleigh, Burkill, & Leakey, 2000). Maximum vertical gradients rather than maximum cellular abundances were used to define the depth at which phytoplankton groups responded strongest to in situ conditions (Figure 2). Under this interpretation, the depth range where abundances changed fastest rather than the single depth where abundances were greatest was chosen to signify the key depth horizon for the distribution of individual phytoplankton groups. This interpretation assumes that the depth of maximum abundance represents the depth of optimal environmental conditions (i.e., light vs. nutrient), whereas the depth of maximum gradient is a region with a strong biological response (e.g., rapid changes to growth or uptake rates (Glibert, 2024) due to rapidly changing environmental conditions such as increased nutrient availability.

2.2.2.3. Calculation of Nutrient Fluxes

Vertical diffusive nutrient fluxes were calculated using Fick's first law, which requires coincident estimates of the vertical nutrient gradient ($\partial N_t/\partial z$), where N_t is a generic nutrient, and z is the depth interval as well as an estimate of the turbulent diffusivity (Kz) (Equation 1).

$$\text{Flux} = -Kz\,\frac{\partial N_t}{\partial z} \tag{1}$$

In this study, the maximum vertical nutrient gradient in nitrate, phosphate, and silicate concentrations is used to provide a per profile estimate of dN/dz. Due to the time constraints imposed on cruise sampling activities, the estimates of Kz have only rarely been measured directly during an AMT cruise. To retrospectively determine diffusive fluxes along each transect, we adopted a two-tier approach to estimating turbulent diffusivities. To begin, a typical oceanic background value of 1×10^{-5} m^2 s^{-1} (0.1 cm^2 s^{-1}; Waterhouse et al., 2014) was used to provide approximate estimates of cross-nutricline nutrient fluxes. Although this background value is comparable to some estimates of open ocean diffusivity (e.g., 0.11 ± 0.02 cm^2 s^{-1}; Ledwell et al., 1993), it is also lower than the mean value reported by Lewis et al. (1986) (3.7×10^{-5} m^2 s^{-1} = 0.3 cm^2 s^{-1}) and does not capture the spatial variability reported by in situ studies (e.g., 0.035–0.187 cm^2 s^{-1} by Painter et al. (2013); 0.1–5 cm^2 s^{-1} by Mouriño-Carballido et al. (2011); 0.3 ± 0.5 cm^2 s^{-1} by Mouriño-Carballido et al. (2021)) with the result that nutrient fluxes calculated using a fixed value for Kz are approximate only (Franks & Inman, 2024; Franks et al., 2021).

To improve upon use of a fixed diffusivity value, Kz was also derived from the local density gradient using the method of Gargett (1984) (Equation 2). This approach has been used successfully in a number of studies for comparable purposes of estimating nutrient fluxes (e.g., Li et al., 2012; Ramsing et al., 1996). Turbulent diffusivity is estimated as

$$Kz = a_0 \sqrt{\frac{1}{N^2}} \tag{2}$$

Where N is the Brunt-Väisälä buoyancy frequency (Equation 3)

$$N = \sqrt{-\frac{g}{\rho}\frac{\partial \rho}{\partial z}} \tag{3}$$

Here, the constant a_o represents the energy input via internal waves and is set equal to 0.001 cm^2 s^{-2} for open ocean conditions (Gargett, 1984), g is the gravitational acceleration constant (9.81 m s^{-2}), ρ is the density at a given depth, and $\frac{\partial \rho}{\partial z}$ is the density gradient over a finite depth interval. Profiles of Kz were calculated using individual density profiles for every CTD cast available from cruises AMT12 to AMT29 (n = 1,396; Table 1). Nutrient fluxes were then estimated using the value of Kz coincident with the vertical nutrient gradient.

2.2.2.4. Consumption of Cross-Nitracline Diffusive Flux (Picoeukaryote Nitrate Uptake)

To estimate where the diffusive nitrate flux is consumed in the euphotic zone, several assumptions related to the consumption of the flux are introduced. First, based upon the phytoplankton distributions (see Section 3), we assume that picoeukaryotes represent a significant proportion of cells located at and above the nitracline and are therefore a significant nitrate consumer.

Second, to estimate picoeukaryote nitrate uptake for a particular depth horizon through which the cross-nitracline flux would pass we assume that this uptake occurs only over the depth interval corresponding to the region of greatest change in abundance (the maximum gradient) and not to the wider depth interval associated with the abundance distribution. We note that cellular abundances appear asymmetrically distributed around the abundance maximum and are rarely distributed with a smooth Gaussian peak. Our assumption implies that only a variable proportion of the picoeukaryote community usually associated with the upper, shallower, part of the abundance peak lying above the nitracline is therefore tasked with consuming the cross-nitracline flux whereas

the lower, deeper, and broader part of the abundance maximum, which lies within the nitracline is excluded (Figure 2). The rationale for this approach is that the lower part of the abundance distribution lies typically within the nitracline and thus lies deeper than the originating horizon used to calculate the nitracline flux.

Third, uptake rates are estimated by taking the interpolated abundances over the maximum gradient depth range, converting abundances from cells ml^{-1} to cells m^{-3} and multiplying abundances by a cellular uptake rate of 0.6 fmol N $cell^{-1}$ h^{-1} (Painter et al., 2014). Picoeukaryote cellular nitrate uptake rates remain poorly constrained with reported half-saturation constants in the range of 150–184 nmol N L^{-1} (Letscher et al., 2023; Painter et al., 2014) and estimates of cellular N uptake ranging 7-fold from ∼0.3 to ∼2 fmol N $cell^{-1}$ h^{-1} (Kang et al., 2017; Painter et al., 2014). Notably, picoeukaryote cellular nitrate uptake rates have been shown to increase with depth (as a function of concentration) from 0.27 fmol NO_3^--N $cell^{-1}$ h^{-1} in nitrate-poor waters above the nitracline to 1.96 fmol NO_3^--N $cell^{-1}$ h^{-1} within the nitrate-rich waters of the nitracline itself (Painter et al., 2014). Although rare, estimates of picoeukaryote cellular NO_3^- uptake appear broadly comparable across environments with the subtropical rates of 0.27–1.96 fmol NO_3^--N $cell^{-1}$ h^{-1} reported by Painter et al. (2014) comparable to rates of ∼0.3–1.4 fmol NO_3^--N $cell^{-1}$ h^{-1} reported by Kang et al. (2017) from the coastal waters of Long Island, USA, at which time surface NO_3^- concentrations were 0.25–0.35 μmol L^{-1} and picoeukaryotes accounted for the majority of NO_3^- uptake by picoplankton. We do not account for variability in the cellular uptake rate, presuming that the rate reported by Painter et al. (2014) represents an appropriate low to mid-range rate under mildly eutrophic conditions (Kang et al., 2017; Painter et al., 2014). Conversion to daily uptake rates was based on the number of daylight hours calculated for each station using the NOAA Solar Calculator (https://gml.noaa.gov/grad/solcalc/), an assumption due to limited available information about the diel periodicity of picoeukaryote NO_3^- uptake, though diel cycles in nutrient uptake are common in phytoplankton and bacterioplankton species (e.g., Cochlan et al., 1991; Kuipers et al., 2000; Probyn et al., 1996). Uptake rates were integrated over the depth range of the maximum picoeukaryote gradient to provide a measure of the daily integrated nitrate demand by that fraction of the picoeukaryote community lying just above the nitracline.

Finally, the efficiency by which picoeukaryotes consume the cross-nitracline flux (the nutrient trap) was estimated simply as the percentage of the diffusive flux consumed within the maximum picoeukaryote gradient depth range.

This approach provides a simple estimate of the magnitude of the nutrient trap based solely upon measured picoeukaryote cellular abundances, an assumed cellular uptake rate, measured local nutrient gradients and derived estimates of local diffusivity and nutrient fluxes.

2.2.2.5. Long-Term (2003–2019) Mean Results

To obtain mean results for the 2003–2019 period (i.e., the long-term mean), all cruise profiles were binned by latitude into 5-degree latitudinal bins to account for the large spatial sampling scales between stations before being averaged to provide estimates of long-term mean values for the Atlantic Ocean. No consideration was made for zonal (east-west) differences in station position, which may contribute to the range of standard errors reported in the results.

3. Results

3.1. Diffusivity Field

Latitudinal cross sections of turbulent diffusivity are shown in Figure 3. Notable features common to all cruises include: (a) high diffusivities (>1 cm^2 s^{-1}) at the southern end of most cruise transects and usually in the upper 100 m, (b) a broad subsurface zone of low diffusivity (<0.1 cm^2 s^{-1}) extending from 50°N to ∼15°S during boreal autumn cruises that deepen toward the south, (c) the reversal and appearance, or possible latitudinal extension, of a similar zone of low diffusivity across the South Atlantic during boreal spring cruises (AMT12, 14, 16), and (d) elevated diffusivities (>0.5 cm^2 s^{-1}) across near-surface depths (<50 m) but discontinuously distributed (i.e., patchy) and most likely attributable to air-sea interactions (Kantha, 2005; D'Asaro, 2013; Thorpe, 2005). Closer examination of the individual sections indicates that the subsurface zone of low diffusivity (Kz < 0.1 cm^2 s^{-1}) observed at ∼100 m depth may oscillate seasonally between the hemispheres. During boreal spring cruises (e.g., AMT12, AMT14, AMT16), the region of low diffusivity shifts or extends southwards across the South Atlantic, whereas during boreal autumn cruises, the zone of low diffusivities is more prevalent across the North Atlantic.

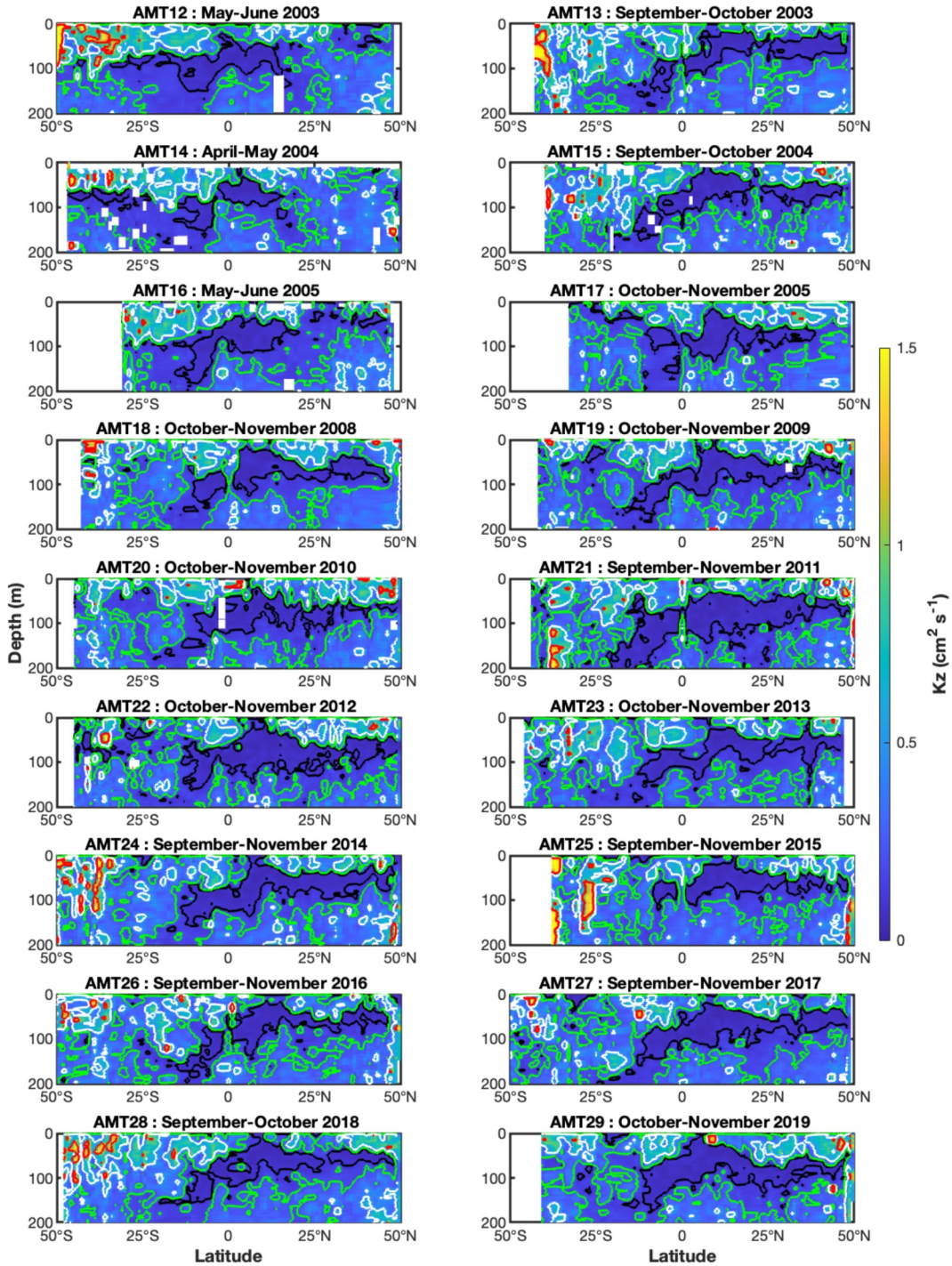

Figure 3. Latitudinal sections of upper ocean (0–200 m) turbulent diffusivities for AMT cruises 12–29. Colored contours denote diffusivities of 0.1 (black), 0.2 (green), 0.5 (white), and 1 (red) cm^2 s^{-1}.

This seasonality, most likely driven by seasonal temperature changes, will ultimately impact diapycnal nutrient fluxes, but the data are temporally inadequate to properly establish formation or destruction of this zone of low diffusivity. Overall, the cross sections indicate a largely quiescent environment with diffusivities that range from 0.06 to 0.35 cm^2 s^{-1} and average 0.17 ± 0.09 cm^2 s^{-1} at the nitracline (Table 2). Comparable diffusivities are found at both the phosphocline and silicicline (Table 2). The results are consistent with general assumptions over the typical magnitude of open ocean diffusivities (e.g., Ledwell et al., 1993; Waterhouse et al., 2014) and with

Journal of Geophysical Research: Biogeosciences 10.1029/2025JG008970

Table 2
Mean Nutricline Gradients, Diffusivities, Nutrient Fluxes, and Molar Flux Ratios Based on AMT Data for the Period 2003–2019

Latitude band	Nitracline (μmol m^{-4})	Phosphocline (μmol m^{-4})	Silicicline (μmol m^{-4})	Nitracline diffusivity (cm^2 s^{-1})	Phosphocline diffusivity (cm^2 s^{-1})	Silicicline diffusivity (cm^2 s^{-1})	NO_3^- flux (μmol m^2 d^{-1})	PO_4^{3-} flux (μmol m^2 d^{-1})	Si flux (μmol m^2 d^{-1})	N:P flux (molar)	N:Si flux (molar)	Si:P flux (molar)
45–50°N	339.7 ± 226.1	28.8 ± 60.2	148.4 ± 331.4	0.17 ± 0.26	0.14 ± 0.11	0.2 ± 0.29	573.2 ± 871.6	32.3 ± 60.5	211.4 ± 372.2	20 ± 12.4	4.4 ± 2.8	7.5 ± 10.9
40–45°N	268.9 ± 221.4	23.5 ± 39.7	68.5 ± 96.4	0.16 ± 0.19	0.18 ± 0.22	0.15 ± 0.13	269.2 ± 184.9	27.9 ± 75.6	89 ± 236.9	18.3 ± 7.2	6.3 ± 7.1	3.9 ± 2.2
35–40°N	209.7 ± 390.3	13.7 ± 40.4	70.7 ± 205.5	0.16 ± 0.08	0.18 ± 0.14	0.17 ± 0.12	345.6 ± 882.5	22.1 ± 59.3	136.2 ± 563.6	20.5 ± 8	4.8 ± 2.5	5.1 ± 2.8
30–35°N	87.7 ± 48	5.1 ± 5.7	23.8 ± 28.5	0.23 ± 0.09	0.25 ± 0.12	0.23 ± 0.12	165.7 ± 111.3	10.7 ± 11.2	39.5 ± 36.1	18.7 ± 7.8	5.3 ± 2.9	4.2 ± 2
25–30°N	85.9 ± 80.3	4.9 ± 6.9	21.8 ± 29.6	0.24 ± 0.11	0.24 ± 0.11	0.21 ± 0.08	170 ± 147.1	9.6 ± 11.7	40 ± 52	21 ± 10.6	5.7 ± 3.4	4.8 ± 3.8
20–25°N	277.2 ± 557.7	21 ± 70.7	119.9 ± 465.2	0.17 ± 0.05	0.2 ± 0.09	0.18 ± 0.07	256.8 ± 366.4	18.2 ± 42.1	98.8 ± 274.6	18.5 ± 7.9	4.4 ± 2.5	5.1 ± 3.4
15–20°N	486.6 ± 452.9	25.5 ± 22.3	98.5 ± 83.3	0.12 ± 0.06	0.12 ± 0.06	0.12 ± 0.06	409 ± 385.1	22.4 ± 20.5	100.1 ± 97.1	19.1 ± 7.7	5 ± 2.8	4.7 ± 2.6
10–15°N	1559.6 ± 1708.9	97.8 ± 132.4	351.7 ± 770.5	0.06 ± 0.04	0.07 ± 0.06	0.07 ± 0.06	751.7 ± 968.1	55.3 ± 126.7	119.3 ± 121.9	18.1 ± 5.1	7.9 ± 11.6	3.7 ± 2.5
5–10°N	825.9 ± 607.3	49.3 ± 35.5	201.1 ± 136.6	0.07 ± 0.05	0.07 ± 0.04	0.08 ± 0.07	480.1 ± 741.9	29.6 ± 42.7	148 ± 229.3	17.3 ± 4.6	4.8 ± 3.3	7 ± 13.9
0–5°N	788.4 ± 523.1	47.5 ± 41.1	247.5 ± 325.4	0.07 ± 0.06	0.08 ± 0.06	0.08 ± 0.07	397 ± 293.7	24.1 ± 18.8	158.3 ± 340.6	18.6 ± 11.3	4 ± 1.5	4.8 ± 2.9
0–5°S	1027.7 ± 1487.4	48.8 ± 39.9	410.2 ± 1164.9	0.08 ± 0.07	0.09 ± 0.09	0.09 ± 0.1	1242.5 ± 4558.1	43.7 ± 102.5	708.6 ± 3345.8	20.6 ± 9.1	3.7 ± 1.2	6.2 ± 5.1
5–10°S	473 ± 192.6	27.7 ± 11.7	120.2 ± 41	0.08 ± 0.04	0.08 ± 0.04	0.08 ± 0.03	335.6 ± 146.3	18 ± 9.8	85.6 ± 39.9	20.3 ± 6.8	4.4 ± 1.8	5.3 ± 2.4
10–15°S	282.2 ± 192.1	21.4 ± 31.3	72.9 ± 28.4	0.11 ± 0.05	0.11 ± 0.03	0.12 ± 0.04	280.5 ± 252.4	21.1 ± 32.7	95.3 ± 45.7	18.2 ± 9.1	3.3 ± 2.8	7.4 ± 4.5
15–20°S	121 ± 42.8	7.6 ± 3.5	37.8 ± 35.5	0.13 ± 0.03	0.16 ± 0.12	0.14 ± 0.05	162.7 ± 54.6	11.7 ± 12	51.9 ± 42.2	18.3 ± 7.1	4.6 ± 5.4	6 ± 6
20–25°S	93.7 ± 152.1	6.1 ± 5.4	28.5 ± 25.8	0.18 ± 0.06	0.19 ± 0.09	0.2 ± 0.1	176.2 ± 390.1	10.8 ± 10.2	49 ± 44.3	17.5 ± 9.9	4.2 ± 3.7	6.8 ± 9.6
25–30°S	87.8 ± 67.1	7.5 ± 5.6	27.9 ± 32.1	0.2 ± 0.07	0.18 ± 0.07	0.22 ± 0.09	156 ± 157.9	11.9 ± 10.9	54 ± 88.9	15.4 ± 8.7	4 ± 2	5.2 ± 4.9
30–35°S	149.8 ± 436.6	10.8 ± 24.1	49.6 ± 84.1	0.21 ± 0.11	0.23 ± 0.1	0.28 ± 0.2	223.2 ± 443.4	21.2 ± 33.9	97.2 ± 131.3	13.9 ± 9.2	3.4 ± 2.5	6.9 ± 9
35–40°S	101.7 ± 63.3	13.3 ± 27.4	30.6 ± 23.2	0.3 ± 0.23	0.46 ± 0.36	0.46 ± 0.31	214.2 ± 161.2	27.6 ± 38.9	101.8 ± 103.5	15.2 ± 12.4	3.7 ± 3	7.2 ± 7.9
40–45°S	245.8 ± 228.3	20.4 ± 18.7	96.6 ± 74	0.22 ± 0.13	0.31 ± 0.27	0.26 ± 0.26	468 ± 607.8	66.8 ± 112.7	184.9 ± 229.2	13.6 ± 7.3	3.3 ± 3.2	5.5 ± 3.6
45–50°S	197.5 ± 209.8	15.7 ± 13.9	105.2 ± 111	0.35 ± 0.25	0.29 ± 0.18	0.35 ± 0.26	552.7 ± 1054.6	46.3 ± 76.2	333.6 ± 500.2	16.4 ± 9.1	2.8 ± 3.3	12.7 ± 18
50–55°S	333.1 ± 249.3	27.3 ± 21.1	518.7 ± 302.5	0.34 ± 0.17	0.4 ± 0.18	0.34 ± 0.17	1045.1 ± 983.7	104.7 ± 82	1829.5 ± 1543.2	15.3 ± 16	0.9 ± 0.9	18 ± 7.8

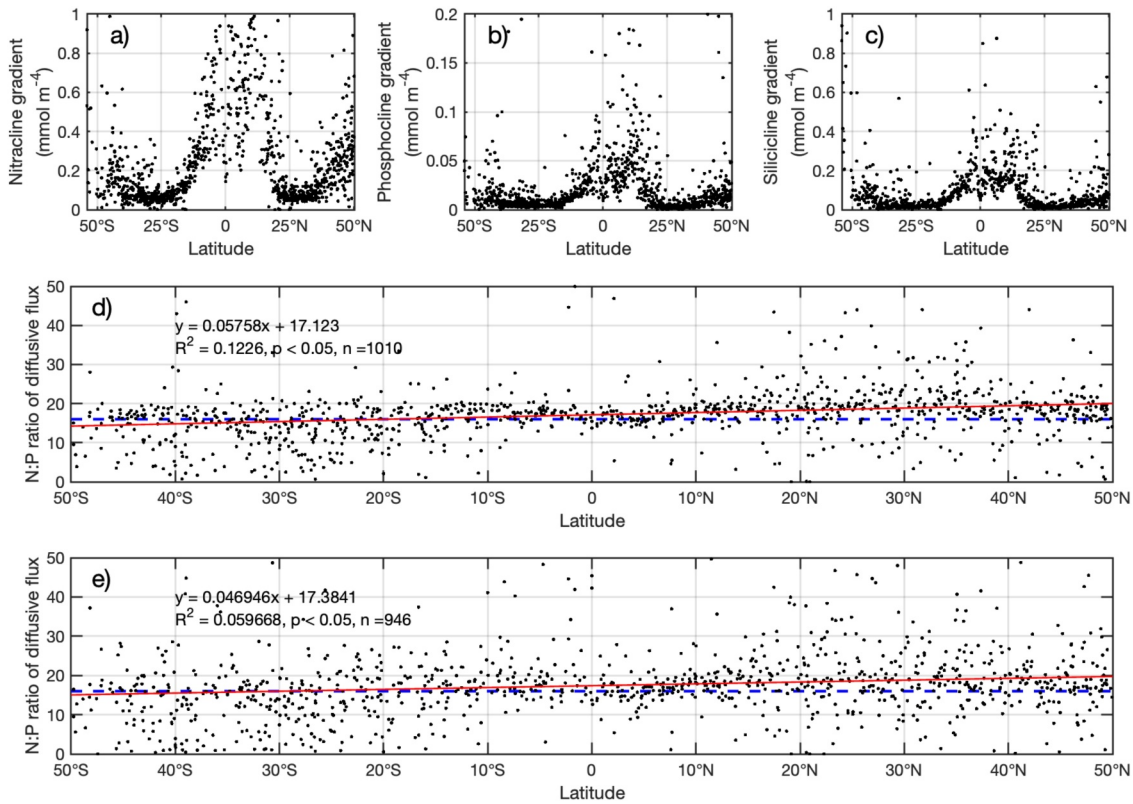

Figure 4. Observed subsurface gradients in (a) nitrate, (b) phosphate, and (c) silicate at the respective nutriclines. Centre panel (d) shows the molar N:P ratio of the vertical diffusive nutrient flux if turbulent diffusivity is assumed constant ($Kz = 0.1$ cm^2 s^{-1}). Lower panel (e) shows the molar N:P ratio of the vertical diffusive nutrient flux when turbulent diffusivity is allowed to vary (Kz values calculated following Gargett, 1984; see Section 2.2). Both fixed and variable diffusive flux estimates reveal a latitudinal gradient with higher molar N:P flux ratios in the North Atlantic. The solid red line represents the fit to the data, the equation of which is presented in the relevant subpanel. The dashed blue line represents the mean global N:P ratio of 16:1.

direct measurements of in situ diffusivities obtained using microstructure shear probes across subtropical regions (e.g., Mouriño-Carballido et al., 2021).

3.2. Nutricline Gradients

Latitudinally binned mean nutricline gradients are presented in Table 2. The general pattern indicated that gradients varied from minima in the center of the subtropical gyres to maxima at the equator with intermediate gradients observed at the northern and southern limits of the transects, a pattern consistent for the individual nitracline, phosphocline, and silicicline gradients (Figure 4). Gradient minima were 85.9 ± 80.3 mmol NO_3^- m^{-4}, 4.9 ± 6.9 mmol PO_4^{3-} m^{-4}, and 21.8 ± 29.6 mmol Si m^{-4} in the North Atlantic (25–30°N) and 87.8 ± 67.1 mmol NO_3^- m^{-4}, 6.1 ± 5.4 mmol PO_4^{3-} m^{-4}, and 27.9 ± 32.1 mmol Si m^{-4} in the South Atlantic (20–30°S). The largest scatter in gradients was located around the equator suggesting significant environmental variability most likely in response to the time-varying intensity of the equatorial upwelling and equatorial current and countercurrents.

3.3. Nutrient Fluxes

Nutrient fluxes mirrored the latitudinal distribution of nutricline gradients with low mean nutrient fluxes in the subtropical gyres and higher nutrient fluxes across the equatorial region (Table 2). Typical minimum fluxes within subtropical latitudes were <170 μmol NO_3^- m^{-2} d^{-1}, ~10 μmol PO_4^{3-} m^{-2} d^{-1}, and 40–50 μmol Si m^{-2} d^{-1} but fluxes increased significantly at the northern and southern ends of the transect.

The corresponding N:P molar flux ratios were more consistent averaging 17.7 ± 8.3 mol:mol between 50°N and 50°S but a statistically significant latitudinal gradient was evident (Figure 4). Consequently, the average N:P ratio

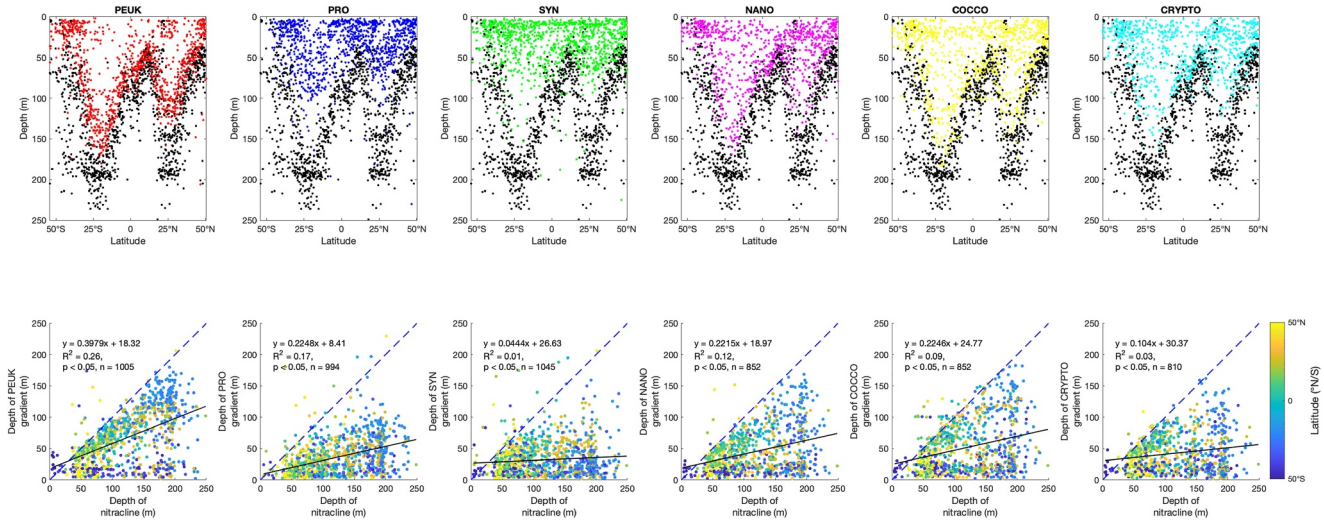

Figure 5. Relationship between the phytoplankton groups resolved by flow cytometry and the nitracline. Top row shows the depth of maximum gradient in phytoplankton abundance (colored dots) and depth of maximum nitrate gradient (black dots). Lower row shows simple regressions between the two variables shown in the top row. Also shown are the 1:1 line (blue dashed line) and a linear fit (black line). Inset equation is for the linear fit.

of the diffusive flux was higher in the North Atlantic (19.3 ± 8.6) than in the South Atlantic (16.6 ± 7.8). Notably, the mean N:P molar flux ratio along much of the transect was close to the Redfield ratio suggesting balanced provision of nutrients via the diffusive pathway.

3.4. Phytoplankton Group Distributions

The vertical gradients associated with each phytoplankton group and their typical association with the nutriclines can be described with one of three distribution types (Figures 5 and 6). For the picoeukaryotes, there was a clear association between the depth of the maximum gradient in abundance and the nitricline with a marginally stronger association to the depth of the maximum phosphate gradient than to the depth of the maximum nitrate gradient (slope was closer to 1). In the lower latitudes, there were typically no surface or intermediate depth gradients in picoeukaryote distributions signifying an almost universal deep association with the nutriclines. Maximum

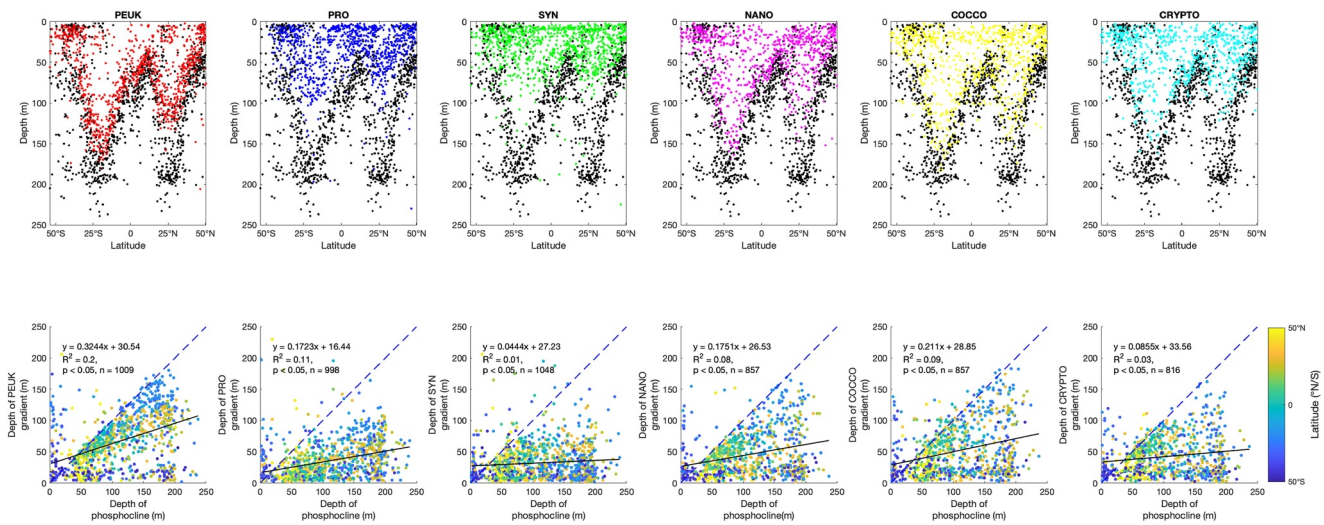

Figure 6. Relationship between the phytoplankton groups resolved by flow cytometry and the phosphocline. Top row shows the depth of maximum gradient in phytoplankton abundance (colored dots) and depth of maximum nitrate gradient (black dots). Lower row shows simple regressions between the two variables shown in the top row. Also shown are the 1:1 line (blue dashed line) and a linear fit (black line). Inset equation is for the linear fit.

Table 3
Mean Nutrient Concentration at Depth of Picoeukaryote Gradient Maximum Averaged by Latitude Based on AMT Data for the Period 2003–2019

Latitude band	NO_3^- (μM)	PO_4^{3-} (μM)	Si (μM)	NO_2^- (μM)
45–50°N	1.1 ± 2.05	0.14 ± 0.15	0.82 ± 0.75	0.02 ± 0
40–45°N	0.61 ± 1.13	0.08 ± 0.08	0.75 ± 0.41	0.06 ± 0.05
35–40°N	0.26 ± 0.52	0.04 ± 0.03	0.73 ± 0.35	0.05 ± 0.07
30–35°N	0.09 ± 0.1	0.03 ± 0.01	0.78 ± 0.16	0.04 ± 0.04
25–30°N	0.09 ± 0.14	0.03 ± 0.01	0.8 ± 0.3	0.03 ± 0.03
20–25°N	0.72 ± 4.35	0.05 ± 0.05	0.73 ± 0.34	0.02 ± 0.01
15–20°N	0.45 ± 0.75	0.1 ± 0.09	1.02 ± 0.46	0.03 ± 0.02
10–15°N	2.37 ± 2.98	0.22 ± 0.19	2.02 ± 0.73	0.05 ± 0.07
5–10°N	1.48 ± 2.59	0.16 ± 0.21	2.08 ± 0.91	0.09 ± 0.1
0–5°N	1.31 ± 2.53	0.17 ± 0.2	1.68 ± 0.87	0.09 ± 0.09
0–5°S	2.2 ± 3.41	0.31 ± 0.27	1.8 ± 1	0.08 ± 0.09
5–10°S	0.48 ± 0.79	0.2 ± 0.12	1.26 ± 0.32	0.08 ± 0.06
10–15°S	0.22 ± 0.56	0.2 ± 0.09	1.09 ± 0.17	0.06 ± 0.07
15–20°S	0.16 ± 0.28	0.2 ± 0.08	1.18 ± 0.61	0.03 ± 0.03
20–25°S	0.18 ± 0.54	0.16 ± 0.07	1.23 ± 0.27	0.03 ± 0.02
25–30°S	0.16 ± 0.46	0.15 ± 0.12	1.3 ± 0.31	0.02 ± 0.02
30–35°S	0.26 ± 0.48	0.14 ± 0.08	1.3 ± 0.64	0.02 ± 0.02
35–40°S	1.81 ± 1.75	0.27 ± 0.17	1.36 ± 0.43	0.03 ± 0.03
40–45°S	5.88 ± 3.01	0.61 ± 0.32	1.53 ± 0.93	0.1 ± 0.08
45–50°S	13.1 ± 6.63	0.99 ± 0.39	4.58 ± 3.83	0.2 ± 0.11
50–55°S	24.38 ± 2.53	1.63 ± 0.25	28.77 ± 13.58	0.29 ± 0.1

picoeukaryote abundances along each transect ranged from 1.3×10^4 (AMT17) to 8.7×10^4 cells ml^{-1} (AMT19), but in the maximum gradient region, abundances were lower and ranged from 1.2×10^3 to 8.4×10^3 cells ml^{-1}.

For *Prochlorococcus* and *Synechococcus* cyanobacteria, the gradient distributions indicated a surface to intermediate depth distribution that was vertically decoupled from the major nutricline gradients. This was particularly evident in the lower latitudes suggesting weaker reliance upon the flux of those nutrients from below. Maximum *Synechococcus* abundances ranged from 3.1×10^4 (AMT12) to 4.6×10^5 cells ml^{-1} (AMT27) and for *Prochlorococcus* the maximum abundances ranged from 1.8×10^5 (AMT12) to 6×10^5 cells ml^{-1} (AMT25).

Lastly, for the nanoplankton, coccolithophores, and cryptophytes, there was an intermediate distribution with some groups being partly associated with the nutriclines and some with shallower intermediate or surface depths. This is interpreted as a mixed response by members of these groups that split between those species favoring an upper ocean high-light low-nutrient regime and those favoring a low-light, high(er)-nutrient regime. Such a distribution is consistent with the presence of "shade-flora," "upper," and "lower" euphotic zone distributions or other such nomenclature used to separate these groups particularly coccolithophores. Fundamentally, however, it demonstrates that a bulk assessment of flow cytometry abundances fails to clearly separate important ecological traits within these groups. Based on the data available, it is not possible to further segregate these phytoplankton groups into high-light or low-light members. Along the transect maximum nanoplankton abundances ranged from 1.8×10^3 cells ml^{-1} (AMT25) to 1.4×10^4 cells ml^{-1} (AMT21), maximum coccolithophore abundances ranged from 52 cells ml^{-1} (AMT25) to 1,360 cells ml^{-1} (AMT21) and maximum cryptophyte abundances ranged from 144 cells ml^{-1} (AMT29) to 1,066 cells ml^{-1} (AMT16). In the following, we exclude a role for the deep living members of these groups due to their low abundances in the depth interval of the maximum picoeukaryote gradient (cryptophytes 50 ± 20 cells ml^{-1}, coccolithophores 20 ± 10 cells ml^{-1}, and nanoflagellates 822 ± 260 cels ml^{-1}).

Between 50°N and 50°S, the average nutrient concentrations associated with the maximum gradient in picoeukaryote abundance were 1.04 ± 1.42 μmol NO_3^- L^{-1}, 0.17 ± 0.14 μmol PO_4^{3-} L^{-1}, 1.26 ± 0.43 μmol Si L^{-1}, and 0.06 ± 0.04 μmol NO_2^- L^{-1} illustrating that picoeukaryotes generally respond to mesotrophic conditions and preferentially lie outside the oligotrophic region of the upper ocean (Table 3). Within the gyres, the associated concentrations were generally lower than the transect averages. For the North Atlantic gyre (20–35°N), the associated concentrations were 0.34 ± 0.3 μmol NO_3^- L^{-1}, 0.05 ± 0.01 μmol PO_4^{3-} L^{-1}, 0.83 ± 0.03 μmol Si L^{-1}, and 0.03 ± 0.01 μmol NO_2^- L^{-1}. The mean molar N:P ratio was therefore 6.8. For the South Atlantic gyre (15–30°S), the concentrations were 0.16 ± 0.01 μmol NO_3^- L^{-1}, 0.18 ± 0.03 μmol PO_4^{3-} L^{-1}, 1.2 ± 0.09 μmol Si L^{-1}, and 0.02 ± 0.01 μmol NO_2^- L^{-1}. The mean molar N:P ratio was ~0.9. Thus, in the South Atlantic picoeukaryote abundances begin to increase at lower in situ nitrate and higher in situ phosphate and silicate concentrations and are associated with considerably lower N:P values than is the case for the North Atlantic. Outside of the gyre latitudes, the associated concentrations are broadly consistent with the average derived for the whole cruise data set (Table 3) except for extreme southern latitudes where the associated concentrations increased rapidly.

3.5. Picoeukaryote Nitrate Uptake

Picoeukaryote nitrate uptake across the abundance maximum gradient region is shown for each cruise in Figure 7 and in aggregate in Figure 8. Maximum volumetric uptake rates per cruise ranged almost 3-fold from 157 μmol NO_3^- m^3 d^{-1} (AMT17) to 453 μmol NO_3^- m^3 d^{-1} (AMT22), but across all cruises, uptake rates were typically <10 μmol NO_3^- m^3 d^{-1} in the North Atlantic subtropical gyre and between 5 and 15 μmol

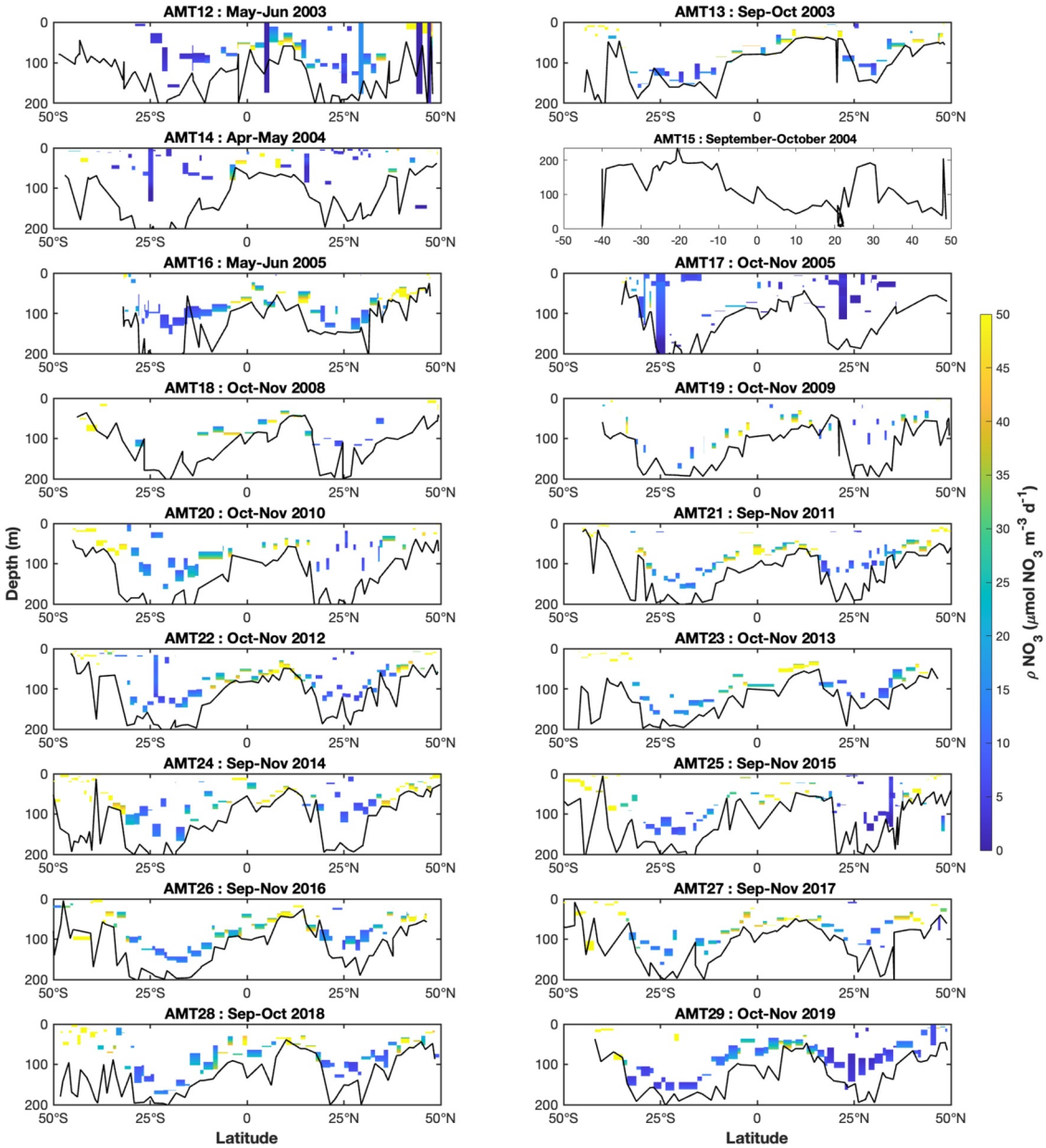

Figure 7. Latitudinal sections showing picoeukaryote nitrate uptake across the region of maximum gradient (picoeukaryote abundance). Whilst this approximation excludes picoeukaryote cells above and below the maximum gradient depth interval, it provides a boundary through which the diapycnal flux originating from the maximum nitrate gradient (black line) must pass and hence a means of estimating the trapping effect.

NO_3^- m^3 d^{-1} in the South Atlantic subtropical gyre. Higher rates exceeding 50 μmol NO_3^- m^3 d^{-1} were obtained for equatorial waters and particularly for the region 10–12°N where uptake appeared to regularly exceed 100 μmol NO_3^- m^3 d^{-1} (Figures 7 and 8). NO_3^- uptake rates integrated across the abundance maximum gradient region ranged from a maximum of 0.9 mmol NO_3^- m^{-2} d^{-1} (AMT23) to 4.6 mmol NO_3^- m^{-2} d^{-1} (AMT12) but across subtropical latitudes were consistently <0.5 mmol NO_3^- m^{-2} d^{-1} (Figure 8). The depth interval for these integrations (i.e., the thickness of the picoeukaryote maximum gradient region) was <30 m for 96% of profiles with the majority (65%) being <10 m.

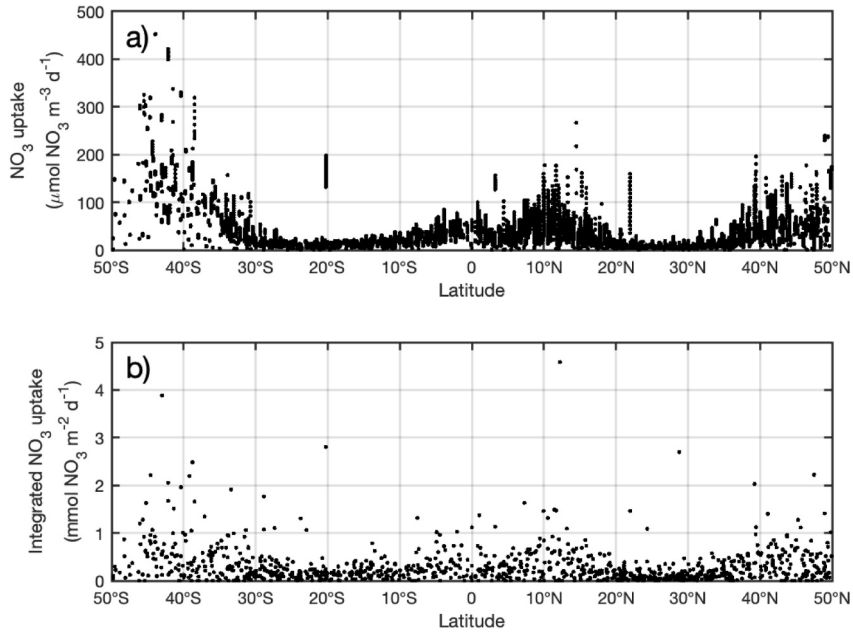

Figure 8. (a) Volumetric picoeukaryote nitrate uptake rates across the abundance maximum gradient region and (b) integrated rates across the abundance maximum gradient region.

3.6. Nutrient Trap

The mean picoeukaryote nutrient trap efficiency is shown for 5° latitudinal bands alongside the mean diffusive nitrate flux and the mean picoeukaryote nitrate demand in Figure 9. Between 50°N and 50°S, the mean nutrient trap shows spatial variability ranging from 65% (15–20°N) to 261% (30–35°S) and averaged 135 ± 65% (Figure 9). This suggests a widespread though variable trapping effect is present throughout the subtropical and tropical latitudes with picoeukaryote nitrate demand likely to regulate, if not inhibit, diapycnal nitrate fluxes to shallower surface waters. Across the North Atlantic subtropical gyre (15–35°N), the trapping efficiency averaged

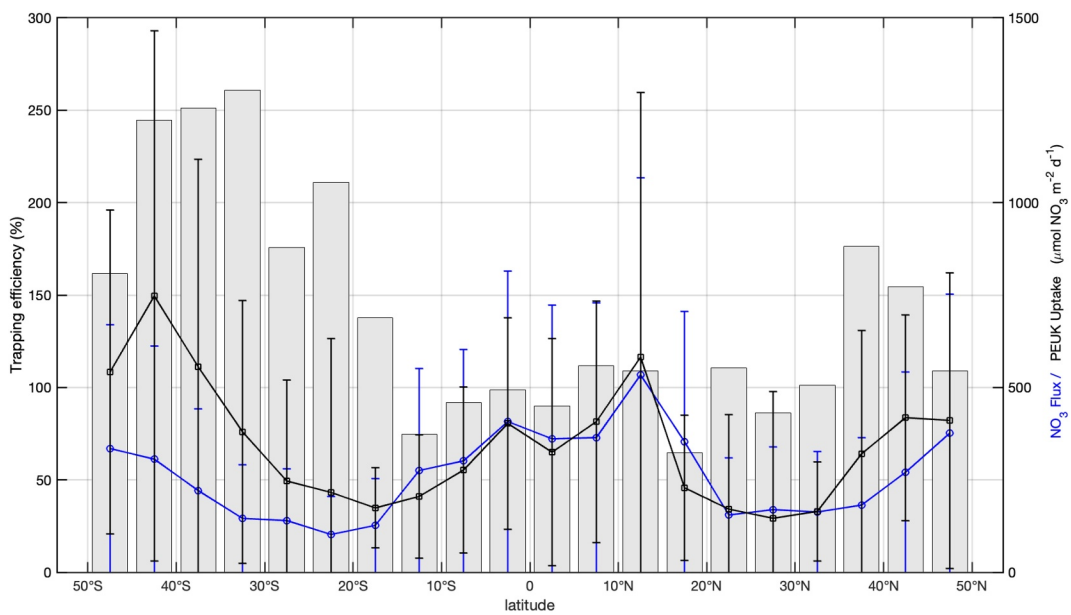

Figure 9. Comparison of the diapycnal NO_3^- flux (blue, right axis), picoeukaryote NO_3^- uptake (black, right axis), and the trapping efficiency (bar charts, left axis) averaged for 2003–2019 (AMT12–AMT29).

99 ± 12% but ranged from 86% to 110% of the diffusive flux across gyre latitudes. In the South Atlantic, larger differences between the diapycnal flux and picoeukaryote demand were evident, and across the South Atlantic subtropical gyre (15–30°S), the trapping efficiency averaged 175 ± 37% but ranged from 137% to 211% of the diffusive flux. Further south (30–35°S), the trapping efficiency reached a transect maximum of 260% of the diffusive flux before decreasing toward the Southern Ocean. The larger trapping effect in the South Atlantic was driven by larger average nitrate demand compared to the North Atlantic (217 vs. 160 μmol NO_3^- m^{-2} d^{-1} respectively) against comparable mean diffusive fluxes in the South Atlantic gyre compared to the North Atlantic (140 vs. 162 μmol NO_3^- m^{-2} d^{-1}, respectively; *t*-test, $p > 0.05$). With respect to the seasonal timing of the underlying cruise observations increased nitrate demand in the South Atlantic coincided with austral spring when irradiances increase toward the summer maximum.

4. Discussion

4.1. Evaluating the Nutrient Trap

The aim of this study was to determine whether autotrophic organisms could capture and remove a significant proportion of the vertical diapycnal nitrate flux thus limiting the significance of this nutrient supply mechanism for productivity across the wider euphotic zone of the subtropical and tropical ocean. More specifically, we asked the question could nitrate-consuming picoeukaryotic phytoplankton, which live at the base of the euphotic zone be significant in isolating the shallower waters of the upper euphotic zone from deep ocean nutrient reservoirs? Based on the analyses presented here the answer is yes: nitrate consumption by only a fraction of the picoeukaryote community may be of sufficient magnitude to consume, and 'trap', most if not all the diffusive nitrate flux at depth (Figure 9). The implications of this are that diapycnal nutrient fluxes are less relevant (or even irrelevant) for supporting productivity and nitrate uptake taking place within waters of the upper euphotic zone several tens of meters above the nitracline. This study complements several previous studies demonstrating that the subtropical euphotic zone is strongly divided into a surface layer with low rates of NO_3^- driven new production and a lower layer with high rates of NO_3^- driven new production (e.g., Coale & Bruland, 1987; Eppley et al., 1988) by illustrating how even the background diffusive nutrient supply pathway can be restricted from reaching surface waters.

Previous investigations have repeatedly shown the widespread occurrence of nanomolar concentrations of nitrate in the subtropical surface ocean (e.g.,Rees et al., 2006; Woodward & Rees, 2001). This persistent state, coupled with near-zero vertical nitrate gradients, has been interpreted as indicating a lack of significant supply from depth (Karl, 2010). Nutrient supply via N_2 fixation is a significant source of new N to the surface ocean (e.g., Benavides & Voss, 2015; Shao et al., 2023; Zehr & Capone, 2021), and it has been demonstrated that in situ nitrification rates are more than capable of accounting for the low nitrate concentrations observed in the surface ocean (Clark et al., 2008, 2021, 2022). This further removes the need for an additional nutrient supply from depth to explain observed nitrate concentrations. In contrast, however, are the growing number of nitrate isotopic observations which consistently indicate that the deep ocean (i.e., sourced from beneath the nitracline) remains the major source of nitrate to the surface ocean (Fripiat et al., 2021; Rafter et al., 2019). This inconsistency is currently unexplained.

Mean picoeukaryote nitrate consumption rates were broadly comparable to estimated NO_3^- fluxes with spatial variability in that balance reflecting known oceanographic and seasonal features (Figure 9). In the South Atlantic, there was a broad region (25–50°S) where picoeukaryote demand exceeded the diffusive supply. As this region was predominantly sampled in austral spring and was therefore likely to be experiencing seasonal deepening of the nitracline due to seasonal increases in irradiance at depth (Letelier et al., 2004), the imbalance between supply and demand most likely drives a seasonal deepening of the nitracline. In the North Atlantic (during boreal autumn), picoeukaryote demand also appeared higher than the diapycnal flux between 35 and 50°N, which may signify the influence of alternative nutrient supply pathways, such as the breakdown of the seasonal thermocline, or an overestimation of the picoeukaryote uptake.

4.2. Limitations and Caveats

Whilst this study has demonstrated that a nutrient trap due to biological consumption at depth can be a significant sink for the diapycnal nitrate flux with implications for marine productivity, the results are nevertheless sensitive to several underlying assumptions.

First, the estimates of in situ diffusivity are derived from profiles of density following the method of Gargett (1984) and do not derive from microstructure shear measurements as has become standard practice. Although the resulting turbulent diffusivities are comparable in magnitude to studies reporting direct observations, it must be acknowledged that the resulting nutrient fluxes can be modified by even slight changes to the diffusivity term. This can be illustrated by use of a "typical" background diffusivity value of 1×10^{-5} m^2 s^{-1}, which produces nutrient fluxes 25% higher than those derived using a variable diffusivity term calculated from the local density field. Notably, several studies have now demonstrated that this background value for mean open ocean diffusivity is often higher than in situ estimates suggesting that its adoption here is unwarranted and that the lower and spatially variable diffusivity values we have calculated, particularly between 25°N and 25°S (Table 2), are more appropriate (e.g., Mouriño-Carballido et al., 2011, 2021; Painter et al., 2013). Alternative approaches to obtain more nuanced predictions of diffusivity in unsampled areas, such as via General Additive Models, indicate that generalized approaches are a promising approach but ultimately still struggle to constrain in situ diffusivity estimates in poorly sampled regions (Mouriño-Carballido et al., 2021). In reality, the diffusivity term is not constant, and whilst efforts to model this term in the absence of in situ observations are developing (Fernandez-Castro et al., 2014; Mouriño-Carballido et al., 2021), it suggests that correct representation of diffusivity in ocean models may be critical for estimating weaker nutrient fluxes. Furthermore, it should be self-evident from Equation 1 that if the diffusivity term is held constant then any diffusive nutrient flux is solely dependent upon the vertical nutrient gradient term. Somewhat unexpectedly, under the scenario of a fixed diffusivity, the stoichiometry of the resulting diffusive nutrient flux was broadly equivalent to the Redfield ratio, whilst also simultaneously exhibiting a latitudinal gradient of increasing N:P flux stoichiometry from south to north (Figure 9). This latitudinal gradient in flux stoichiometry is in turn driven by the vertical gradients in nitrate and phosphate with indications that it is the proportionately larger reduction in phosphocline gradient (~18%), rather than the nitracline gradient (~2%), between the South and North Atlantic that is responsible for this gradient (as estimated from gradient minima shown in Table 3). The presence of this latitudinal gradient implies more N than P (relative to Redfield) is supplied to the North Atlantic, which agrees with the broad consensus that the North Atlantic is more strongly P-limited than the South Atlantic (Mather et al., 2008; Moore, 2016; Moore et al., 2013).

Second, a simplistic scaling argument was adopted to estimate picoeukaryote nitrate demand from picoeukaryote cellular abundances. Estimates of the picoeukaryote half saturation constant for N are limited but appear comparable (150–184 nmol; Letscher et al., 2023; Painter et al., 2014). Under mesotrophic conditions, cellular NO_3^- uptake was reported to average 0.6 fmol N $cell^{-1}$ h^{-1} (Painter et al., 2014). Here, this scaling factor of 0.6 fmol N $cell^{-1}$ h^{-1} was used to convert cellular abundances to in situ NO_3^- uptake under the assumption that the cellular N uptake rate remained constant. A focus on that fraction of the picoeukaryote community lying above the nitracline and within a narrow depth range (typically <30 m thick) designated by where the greatest change in abundance occurred (the maximum gradient), limited the potential overestimation of picoeukaryote NO_3^- uptake by omitting picoeukaryote cells living deeper within the eutrophic nitracline or higher within the oligotrophic water column. Logically, although the assimilatory actions of cells within the nitracline influence the local nitracline gradient, ultimately controlling the magnitude of the diffusive flux, they do not subsequently consume any nutrient flux that leaves the nitracline region, which can only be consumed by cells living at shallower depths. For reasons of simplicity, the region of the maximum gradient in abundance was chosen rather than considering the entire picoeukaryote community found above the nitracline because observations suggest that cellular uptake rates remain depressed away from the nitracline and begin to increase as the nitracline is approached (Painter et al., 2014) most likely as a function of nutrient affinity (Fawcett et al., 2011; Flombaum et al., 2020). More simply, as the nutrient trap can be conceptualized as being due to the actions of cells acting on the vertical flux passing into a defined layer of the water column, it follows that cells outside of this zone contribute less (or nothing) to that estimate of consumption. To assess the sensitivity our results to the choice of cellular uptake rate, we examined scenarios where a lower rate of 0.3 and an upper rate of 2 fmol N $cell^{-1}$ h^{-1} were used with these rates representing the lower and upper limits reported by Painter et al. (2014) and Kang et al. (2017). For a lower cellular uptake rate of 0.3 fmol N $cell^{-1}$ h^{-1}, the trapping efficiency decreased to ~50% along the transect between 15°S and 50°N and to ~100% between 15°S and 50°S. Along much of the transect therefore the diffusive NO_3^- flux exceeded the cumulative picoeukaryote uptake rate leading to a net flux to the upper surface ocean. For the upper rate of 2 fmol N $cell^{-1}$ h^{-1}, the trapping efficiency exceeded 200% everywhere reaching over 700% at 35°S. Uptake therefore grossly exceeded the diffusive NO_3^- flux. This suggests that a trapping efficiency of 50%–100% can be expected even under conditions of low picoeukaryote cellular uptake (0.3–0.6 fmol N $cell^{-1}$ h^{-1}). For the chosen cellular rate of 0.6 fmol NO_3^- cell hr^{-1}, we find that

uptake broadly balances the flux with a trapping efficiency of ~100% along much of the transect except for the far southern end (Figure 9). At its simplest a rate of 0.6 fmol NO_3^- cell hr^{-1} leads to an efficient nutrient trap.

Third, although the results indicate a consistent environment across multiple years with mean diffusivity rates (0.17–0.20 $cm^2\ s^{-1}$), diapycnal fluxes (140–162 μmol N $m^{-2}\ d^{-1}$), and uptake rates (160–217 μmol NO_3^- $m^{-2}\ d^{-1}$) resulting in significant trapping (99%–175%) in the central gyre regions, the inter-gyre differences evident in the results represent mean seasonal conditions only due to the limitations of cruise timings. True seasonality is not captured via annual cruises and the expected seasonal changes in nitracline depth and gradient within a gyre (Letelier et al., 2004) is not evident here. This means that the results are reflective of the boreal autumn period for the North Atlantic and austral spring for the South Atlantic during which time picoeukaryotes in the South Atlantic appear to trap a greater proportion of the nitrate flux than in the North Atlantic. Consequently, the greater magnitude of the trapping effect reported for the South Atlantic (>100% of the diffusive flux) cannot be considered representative of annual conditions and it is highly likely, though not demonstrated here, that the trapping efficiency in the South Atlantic reduces in magnitude during the austral autumn months as irradiance weakens at depth thus allowing more nutrients to diffuse upwards toward the surface. This "see-saw" motion of the nitracline has been demonstrated from long-term observations at a fixed location in the North Pacific (Letelier et al., 2004) but not yet at basin scales. It is likely to become increasingly apparent, however, with the growth of the BioGeoChemical-Argo array (Biogeochemical-Argo Planning Group, 2016) and increased observations of the nitracline region will likely resolve this key seasonality of the subsurface nitrate gradients (Johnson et al., 2010, 2013).

Fourth, the picoeukaryote group, defined operationally as eukaryotic cells <2 μm in size, consists of multiple taxonomic groups (e.g., *Prasinophyceae*, *Pelagophyceae*, *Cryptophyceae*, *Prymnesiophyceae*; Worden & Not, 2008), each with their own particular environmental requirements. Current flow cytometry methodologies do not discriminate these taxonomic identities, but detailed genetic sequencing indicates changes to picoeukaryote diversity and trophic function with depth and a prevalence for the autotrophic *Pelagophyceae*, *Mamiellophyceae*, *Cryptomonadales*, and heterotrophic *Telonema* groups at the deep chlorophyll maximum (Giner et al., 2020). Recognition of, and accounting for, this taxonomic diversity when estimating the nutrient trap effect is outside of current capabilities but should be explored in future. The inclusion of a specific picoeukaryote group in Earth System Models is not yet widespread whilst inclusion of taxonomic diversity is beyond current model capabilities but may be a promising developmental step.

4.3. Implications

Efforts to understand how changes in nutrient supply in a warming world may impact low-latitude productivity have highlighted the role of stratification (Bopp et al., 2013). Whist predictions of a warmer more stratified ocean are broadly linked to reduced nutrient supply and to a long-term decrease in subtropical ocean productivity, there is no clear inclusion of a biological trapping effect in such predictions. This is significant because whilst increased temperatures will increase stratification with the potential to reduce nutrient fluxes, higher temperatures also enhance metabolic processes, which, in the case of picoeukaryotes, may result in increased demand for nitrate and higher overall productivity. It is notable that one recent study has already highlighted that the global fraction of net primary production occurring at depth is increasing (Silsbe et al., 2025). High nitrate uptake potential at depth directly shapes the local nitracline gradient, ultimately impacting the magnitude of diapycnal nutrient fluxes. Furthermore, high uptake potential also increases the consumption of the cross-nitracline flux further restricting the significance of diapycnal nutrient fluxes to a lower subsection of the water column immediately above the nitracline, thereby reducing supply to the entire water column with implications for the association between diapycnal fluxes and new or primary production generally. As models currently consider diffusive nutrient fluxes into the euphotic zone as an important factor supporting productivity, omitting or poorly representing this strong biological control on the diapycnal flux likely means that such fluxes are overestimated in significance and impact. Finally, Although it is now recognized that zooplankton grazing rates are increased by warming temperature trends, thus contributing to the decline in low-latitude marine productivity (Laufkötter et al., 2015), the explicit inclusion of other biological processes sensitive to ambient temperatures and impacting productivity rates, such as picoeukaryote growth rates, are not explicitly resolved in many models. Such temperature-sensitive processes may also contribute significantly to projected trends in primary production.

5. Conclusions

A test of the nutrient trap hypothesis finds that (a) demand for nitrate in the waters immediately above the nitracline traps the diapycnal flux at depth, thereby greatly reducing the relevance of diapycnal fluxes for productivity across the wider euphotic zone, and (b) diapycnal nutrient fluxes are influenced by phytoplankton demand for nitrate at the nitracline, which shapes local nitracline gradients and hence controls the magnitude of diapycnal fluxes. It is suggested that diapycnal nutrient fluxes are only weakly relevant to global model projections of how primary production may change in the low-latitude ocean under a warmer, more stratified, future. Such projections typically consider the whole euphotic zone and improvements in tracking where nutrients are consumed within subsections of the euphotic zone may lead to greater insight into how future ocean productivity may be shaped by warmer waters.

Conflict of Interest

The authors declare no conflicts of interest relevant to this study.

Data Availability Statement

All data collected during the Atlantic Meridional Transect program are hosted at the British Oceanographic Data Centre (https://www.bodc.ac.uk). Data sets can be freely accessed via a search of the BODC database (https://www.bodc.ac.uk/data/), obtained via the Published Data Library (https://www.bodc.ac.uk/data/published_data_library/), or in a minority of cases are available upon direct request to BODC. See Tables S1–S3 in Supporting Information S1 for further details. Data utilized in this study come from Ayliffe (2020), Ballard and Becker (2022), Bargery (2021a, 2021b), Harris and Rees (2016), Harris and Woodward (2014), Painter (2017), Painter et al. (2017), Tarran (2020a, 2020b), Tarran and May (2020a, 2020b), Tarran and Zubkov (2020a, 2020b, 2020c, 2020d, 2020e, 2020f, 2020g, 2020h, 2020i), Tarran et al. (2020), Thomas (2016, 2017a, 2017b, 2021), Woodward and Beesley (2022), Woodward and Harris (2015, 2019a, 2019b, 2022a, 2022b, 2022c), and Woodward et al. (2018, 2021).

Acknowledgments

Since its inception the AMT program (www.amt-uk.org) has been funded by the UK Natural Environment Research Council (NERC). It is currently funded by the UK Natural Environment Research Council through its National Capability Long-term Single Centre Science Program, Atlantic Climate and Environmental Strategic Science—AtlantiS (Grant NE/Y005589/1). This study contributes to the international IMBeR project and is contribution number 422 of the AMT program. SP wishes to thank the many individual researchers involved with the AMT program who have helped in the collection of significant quantities of data since 1995. Further details about the individual data sets used in this study are available via original publications (www.amt-uk.org/publications/). We thank the editors and three anonymous reviewers for their comments which helped improve this study.

References

Aiken, J., & Bale, A. J. (2000). An introduction to the Atlantic Meridional Transect (AMT) Programme. *Progress in Oceanography*, *45*(3–4), 251–256. https://doi.org/10.1016/s0079-6611(00)00004-5

Anderson, G. C. (1969). Subsurface chlorophyll maximum in the Northeast Pacific Ocean. *Limnology & Oceanography*, *14*(3), 386–391. https://doi.org/10.4319/lo.1969.14.3.0386

Armstrong, F. A. J., Stearns, C. A., & Strickland, J. D. H. (1967). The measurement of upwelling and subsequent biological processes by means of the Technicon Autoanalyser and associated equipment. *Deep-Sea Research*, *14*(3), 381–389. https://doi.org/10.1016/0011-7471(67)90082-4

Ayliffe, J. O. (2020). AMT26 (JR16001) CTD profiles (pressure, temperature, salinity, potential temperature, density, fluorescence, transmittance, downwelling PAR, dissolved oxygen concentration) calibrated and binned to 1 dbar [Dataset]. *British Oceanographic Data Centre, National Oceanography Centre, NERC, UK*. https://doi.org/10.5285/aa51baf6-2095-6c28-e053-6c86abc0d7f7

Baker, A. R., Adams, C., Bell, T. G., Jickells, T. D., & Ganzeveld, L. (2013). Estimation of atmospheric nutrient inputs to the Atlantic Ocean from 50°N to 50°S based on large-scale field sampling: Iron and other dust-associated elements. *Global Biogeochemical Cycles*, *27*(3), 755–767. https://doi.org/10.1002/gbc.20062

Baker, A. R., Jickells, T. D., Biswas, K. F., Weston, K., & French, M. (2006). Nutrients in atmospheric aerosol particles along the Atlantic Meridional Transect. *Deep-Sea Research Part II*, *53*(14–16), 1706–1719. https://doi.org/10.1016/j.dsr2.2006.05.012

Baker, A. R., Kelly, S. D., Biswas, K. F., Witt, M., & Jickells, T. D. (2003). Atmospheric deposition of nutrients to the Atlantic Ocean. *Geophysical Research Letters*, *30*(24), 2296. https://doi.org/10.1029/2003gl018518

Baker, A. R., Weston, K., Kelly, S. D., Voss, M., Streu, P., & Cape, J. N. (2007). Dry and wet deposition of nutrients from the tropical Atlantic atmosphere: Links to primary productivity and nitrogen fixation. *Deep-Sea Research Part I*, *54*(10), 1704–1720. https://doi.org/10.1016/j.dsr.2007.07.001

Ballard, J. R., & Becker, S. M. (2022). Atlantic Meridional Transect cruise AMT28 (JR18001) micro-molar nutrient measurements from CTD bottle samples collected in 2018 [Dataset]. *NERC EDS British Oceanographic Data Centre NOC*. https://doi.org/10.5285/c73b01f0-c019-4312-e053-6c86abc08369

Banse, K. (1987). Clouds, deep chlorophyll maxima and the nutrient supply to the mixed layer of stratified water bodies. *Journal of Plankton Research*, *9*(5), 1031–1036. https://doi.org/10.1093/plankt/9.5.1031

Bargery, A. (2021a). JR20131005 (AMT23, JR300) CTD profiles (pressure, temperature, salinity, potential temperature, density, fluorescence, transmissance, downwelling PAR, dissolved oxygen concentration) calibrated and binned to 1 dbar [Dataset]. *NERC EDS British Oceanographic Data Centre NOC*. https://doi.org/10.5285/c0152486-cdad-4744-e053-6c86abc050c2

Bargery, A. (2021b). JR15001 (AMT25, JR864) CTD profiles (pressure, temperature, salinity, potential temperature, density, fluorescence, transmissance, downwelling PAR, dissolved oxygen concentration) calibrated and binned to 1 dbar [Dataset]. *NERC EDS British Oceanographic Data Centre NOC*. https://doi.org/10.5285/c0152486-cdaf-4744-e053-6c86abc050c2

Benavides, M., & Voss, M. (2015). Five decades of N2 fixation research in the North Atlantic Ocean. *Frontiers in Marine Science*, *2*, 40. https://doi.org/10.3389/fmars.2015.00040

Bernhardt, H., & Wilhelms, A. (1967). The continuous determination of low level iron, soluble phosphate and total phosphate with the Auto-Analyzer. In *Technicon Symposia* (Vol. 1, pp. 385–389).

Biogeochemical-Argo Planning Group. (2016). In K. Johnson & H. Claustre (Eds.), *The scientific rationale, design and Implementation Plan for a Biogeochemical-Argo float array*. https://doi.org/10.13155/46601

Bopp, L., Resplandy, L., Orr, J. C., Doney, S. C., Dunne, J. P., Gehlen, M., et al. (2013). Multiple stressors of ocean ecosystems in the 21st century: Projections with CMIP5 models. *Biogeosciences*, *10*(10), 6225–6245. https://doi.org/10.5194/bg-10-6225-2013

Brewer, P. G., & Riley, J. P. (1965). The automatic determination of nitrate in seawater. *Deep-Sea Research*, *12*(6), 765–772. https://doi.org/10.1016/0011-7471(65)90797-7

Clark, D. R., Rees, A. P., Ferrera, C., Al-Moosawi, L., Somerfield, P. J., Harris, C., et al. (2021). Nitrification in the oligotrophic Atlantic Ocean. *Biogeosciences Discussions*. https://doi.org/10.5194/bg-2021-5184

Clark, D. R., Rees, A. P., Ferrera, C. M., Al-Moosawi, L., Somerfield, P. J., Harris, C., et al. (2022). Nitrite regeneration in the oligotrophic Atlantic Ocean. *Biogeosciences*, *19*(5), 1355–1376. https://doi.org/10.5194/bg-19-1355-2022

Clark, D. R., Rees, A. P., & Joint, I. (2008). Ammonium regeneration and nitrification rates in the oligotrophic Atlantic Ocean: Implications for new production estimates. *Limnology & Oceanography*, *53*(1), 52–62. https://doi.org/10.4319/lo.2008.53.1.0052

Coale, K. H., & Bruland, K. W. (1987). Oceanic stratified euphotic zone as elucidated by ^{234}Th:^{238}U disequilibria. *Limnology & Oceanography*, *32*(1), 189–200. https://doi.org/10.4319/lo.1987.32.1.0189

Cochlan, W. P., Harrison, P. J., & Denman, K. L. (1991). Diel periodicity of nitrogen uptake by marine phytoplankton in nitrate-rich environments. *Limnology & Oceanography*, *36*(8), 1689–1700. https://doi.org/10.4319/lo.1991.36.8.1689

D'Asaro, E. A. (2013). Turbulence in the upper-ocean mixed layer. *Annual Review of Marine Science*, *6*(1), 101–115. https://doi.org/10.1146/annurev-marine-010213-135138

Eppley, R. W., Swift, E., Redalje, D. G., Landry, M. R., & Haas, L. W. (1988). Subsurface chlorophyll maximum in August-September 1985 in the CLIMAX area of the North Pacific. *Marine Ecology Progress Series*, *42*, 289–301. https://doi.org/10.3354/meps042289

Fawcett, S. E., Lomas, M. W., Casey, J. R., Ward, B. B., & Sigman, D. M. (2011). Assimilation of upwelled nitrate by small eukaryotes in the Sargasso Sea. *Nature Geoscience*, *4*(10), 717–722. https://doi.org/10.1038/ngeo1265

Fernandez-Castro, B., Mouriño-Carballido, B., Benítez-Barrios, V. M., Chouciño, P., Fraile-Nuez, R., Graña, R., et al. (2014). Microstructure turbulence and diffusivity parameterization in the tropical and subtropical Atlantic, Pacific and Indian Oceans during the Malaspina 2010 expedition. *Deep-Sea Research Part I*, *94*, 15–30.

Fernandez-Gonzalez, C., Tarran, G. A., Schuback, N., Woodward, E. M. S., Aristegui, J., & Maranon, E. (2022). Phytoplankton responses to changing temperature and nutrient availability are consistent across the tropical and subtropical Atlantic. *Communications Biology*, *5*(1), 1035. https://doi.org/10.1038/s42003-022-03971-z

Flombaum, P., Wang, W.-L., Primeau, F. W., & Martiny, A. C. (2020). Global picophytoplankton niche partitioning predicts overall positive response to ocean warming. *Nature Geoscience*, *13*(2), 116–120. https://doi.org/10.1038/s41561-019-0524-2

Franks, P. J. S., & Inman, B. G. (2024). Shortcomings of the dissipation rate for understanding the turbulent environment of plankton—And a potential solution. *Limnology & Oceanography*, *69*(S1). https://doi.org/10.1002/lno.12501

Franks, P. J. S., Inman, B. G., MacKinnon, J. A., Alford, M. H., & Waterhouse, A. F. (2021). Oceanic turbulence from a planktonic perspective. *Limnology & Oceanography*, *67*(2), 348–363. https://doi.org/10.1002/lno.11996

Fripiat, F., Martínez-García, A., Marconi, D., Fawcett, S. E., Kopf, S. H., Luu, V. H., et al. (2021). Nitrogen isotopic constraints on nutrient transport to the upper ocean. *Nature Geoscience*, *14*(11), 855–861. https://doi.org/10.1038/s41561-021-00836-8

Gargett, A. E. (1984). Vertical eddy diffusivity in the ocean interior. *Journal of Marine Research*, *42*(2), 359–393. https://doi.org/10.1357/002224084788502756

Giner, C. R., Pernice, M. C., Balague, V., Duarte, C. M., Gasol, J. M., Logares, R., & Massana, R. (2020). Marked changes in diversity and relative activity of picoeukaryotes with depth in the world ocean. *ISME Journal*, *14*(2), 437–449. https://doi.org/10.1038/s41396-019-0506-9

Glibert, P. M. (2024). *Phytoplankton whispering: An introduction to the physiology and ecology of Microalgae* (p. 753). Springer.

Grasshoff, K. (1976). *Methods of seawater AnalysisWeinheim*. Verlag Chemie.

Harris, C., & Rees, A. P. (2016). AMT19 (JC039) micro-molar nutrient measurements from CTD bottle samples [Dataset]. *British Oceanographic Data Centre - Natural Environment Research Council, UK*. https://doi.org/10.5285/42974c1c-ea2d-57a5-e053-6c86abc09d06

Harris, C., & Woodward, E. M. S. (2014). AMT20 (JC053) micro-molar nutrient measurements from CTD bottle samples [Dataset]. *British Oceanographic Data Centre - Natural Environment Research Council, UK*. https://doi.org/10.5285/f3c482e3-245e-36a5-e044-000b5de50f38

Hopkinson, C. S., Jr., Vallino, J. J., & Nolin, A. (2002). Decomposition of dissolved organic matter from the continental margin. *Deep-Sea Research II*, *49*(20), 4461–4478. https://doi.org/10.1016/s0967-0645(02)00125-x

Hopkinson, C. S., Jr., Fry, B., & Nolin, A. L. (1997). Stoichiometry of dissolved organic matter dynamics on the continental shelf of the northeastern U.S.A. *Continental Shelf Research*, *17*(5), 473–489. https://doi.org/10.1016/s0278-4343(96)00046-5

Hopkinson, C. S., & Vallino, J. J. (2005). Efficient export of carbon to the deep ocean through dissolved organic matter. *Nature*, *433*(7022), 142–145. https://doi.org/10.1038/nature03191

Jamart, B. M., Winter, D. F., Banse, K., Anderson, G. C., & Lam, R. K. (1977). A theoretical study of phytoplankton growth and nutrient distribution in the Pacific ocean off the northwestern U.S. coast. *Deep-Sea Research*, *24*(8), 753–773. https://doi.org/10.1016/0146-6291(77)90498-2

Jickells, T. D., Baker, A. R., & Chance, R. (2016). Atmospheric transport of trace elements and nutrients to the oceans. *Philosophical Transactions of the Royal Society A*, *374*(2081), 20150286. https://doi.org/10.1098/rsta.2015.0286

Johnson, K. S., Coletti, L., Jannasch, H., Sakamoto, C., Swift, D., & Riser, S. (2013). Long-term nitrate measurements in the ocean using the In Situ Ultraviolet Spectrophotometer: Sensor integration into the Apex profiling float. *Journal of Atmospheric and Oceanic Technology*, *30*(8), 1854–1866. https://doi.org/10.1175/jtech-d-12-00221.1

Johnson, K. S., Riser, S. C., & Karl, D. M. (2010). Nitrate supply from deep to near-surface waters of the North Pacific subtropical gyre. *Nature*, *465*(7301), 1062–1065. https://doi.org/10.1038/nature09170

Junger, P. C., Sarmento, H., Giner, C. R., Mestre, M., Sebastián, M., Morán, X. A. G., et al. (2023). Global biogeography of the smallest plankton across ocean depths. *Science Advances*, *9*(45), eadg9763. https://doi.org/10.1126/sciadv.adg9763

Kang, Y., Kudela, R. M., & Gobler, C. J. (2017). Quantifying nitrogen assimilation rates of individual phytoplankton species and plankton groups during harmful algal blooms via sorting flow cytometry. *Limnology and Oceanography: Methods*, *15*(8), 706–721. https://doi.org/10.1002/lom3.10193

Kantha, L. (2005). The surface mixed layer: An overview *in* Marine Turbulence. In H. Z. Baumert, J. H. Simpson, & J. Sündermann (Eds.), *Theories, observations and models. Results of the CARTUM project*. Cambridge University Press.

Karl, D. M. (2010). Oceanic ecosystem time-series programs: Ten lessons learned. *Oceanography*, *23*(3), 104–125. https://doi.org/10.5670/oceanog.2010.27

Karl, D. M., Letelier, R. M., Bidigare, R. R., Björkman, K. M., Church, M. J., Dore, J. E., & White, A. E. (2021). Seasonal-to-decadal scale variability in primary production and particulate matter export at Station ALOHA. *Progress in Oceanography*, *195*, 102563. https://doi.org/10.1016/j.pocean.2021.102563

Kirkwood, D. S. (1989). Simultaneous determination of selected nutrients in seawater. In *Contribution to Hydrography Committee, C.M.1989/C: 29, Ref. E* (p. 12). The Hague, International Council for the Exploration of the Sea.

Kuipers, B., van Noort, G. J., Vosjan, J., & Herndl, G. J. (2000). Diel periodicity of bacterioplankton in the euphotic zone of the subtropical Atlantic Ocean. *Marine Ecology Progress Series*, *201*, 13–25. https://doi.org/10.3354/meps201013

Latasa, M., Cabello, A. M., Moran, X. A. G., Massana, R., & Scharek, R. (2017). Distribution of phytoplankton groups within the deep chlorophyll maximum. *Limnology & Oceanography*, *62*(2), 665–685. https://doi.org/10.1002/lno.10452

Laufkötter, C., Vogt, M., Gruber, N., Aita-Noguchi, M., Aumont, O., Bopp, L., et al. (2015). Drivers and uncertainties of future global marine primary production in marine ecosystem models. *Biogeosciences*, *12*(23), 6955–6984. https://doi.org/10.5194/bg-12-6955-2015

Ledwell, J. R., Watson, A. J., & Law, C. S. (1993). Evidence for slow mixing across the pycnocline from an open-ocean tracer-release experiment. *Nature*, *364*(6439), 701–703. https://doi.org/10.1038/364701a0

Letelier, R., Karl, D. M., Abbott, M. A., & Bidigare, R. R. (2004). Light driven seasonal patterns of chlorophyll and nitrate in the lower euphotic zone of the North Pacific Subtropical Gyre. *Limnology & Oceanography*, *49*(2), 508–519. https://doi.org/10.4319/lo.2004.49.2.0508

Letscher, R. T., Moore, J. K., Martiny, A. C., & Lomas, M. W. (2023). Biodiversity and stoichiometric plasticity increase pico-phytoplankton contributions to marine net primary productivity and the biological pump. *Global Biogeochemical Cycles*, *37*(8), e2023GB007756. https://doi.org/10.1029/2023gb007756

Lewis, M. R., Harrison, W. G., Oakey, N. S., Herbert, D., & Platt, T. (1986). Vertical nitrate fluxes in the oligotrophic ocean. *Science*, *234*(4778), 870–873. https://doi.org/10.1126/science.234.4778.870

Li, X. N., Taylor, G. T., Astor, Y., Varela, R., & Scranton, M. I. (2012). The conundrum between chemoautotrophic production and reductant and oxidant supply: A case study from the Cariaco Basin. *Deep Sea Research Part I: Oceanographic Research Papers*, *61*, 1–10. https://doi.org/10.1016/j.dsr.2011.11.001

Lonborg, C. (2009). *Bioavailability of dissolved organic matter in coastal waters* (p. 163). University of Aberdeen, University of Aberdeen. PhD.

Mahaffey, C., Michaels, A. F., & Capone, D. G. (2005). The conundrum of marine N_2 fixation. *American Journal of Science*, *305*(6–8), 546–595. https://doi.org/10.2475/ajs.305.6-8.546

Mather, R. L., Reynolds, S. E., Wolff, G. A., Williams, R. G., Torres-Valdes, S., Woodward, E. M. S., et al. (2008). Phosphorus cycling in the North and South Atlantic Ocean subtropical gyres. *Nature Geoscience*, *1*(7), 439–443. https://doi.org/10.1038/ngeo232

Moore, C. M. (2016). Diagnosing oceanic nutrient deficiency. *Philosophical Transactions of the Royal Society A*, *374*(2081), 20150290. https://doi.org/10.1098/rsta.2015.0290

Moore, C. M., Mills, M. M., Achterberg, E. P., Geider, R. J., LaRoche, J., Lucas, M. I., et al. (2009). Large-scale distribution of Atlantic nitrogen fixation controlled by iron availability. *Nature Geoscience*, *2*(12), 867–871. https://doi.org/10.1038/ngeo667

Moore, C. M., Mills, M. M., Arrigo, K. R., Berman-Frank, I., Bopp, L., Boyd, P. W., et al. (2013). Processes and patterns of oceanic nutrient limitation. *Nature Geoscience*, *6*(9), 701–710. https://doi.org/10.1038/ngeo1765

Mouriño-Carballido, B., Grana, R., Fernandez, A., Bode, A., Varela, M., Dominguez, J. F., et al. (2011). Importance of N_2 fixation vs. nitrate eddy diffusion along a latitudinal transect in the Atlantic Ocean. *Limnology & Oceanography*, *56*(3), 999–1007. https://doi.org/10.4319/lo.2011.56.3.0999

Mouriño-Carballido, B., Hojas, E., Cermeno, P., Choucino, P., Fernandez-Castro, B., Latasa, M., et al. (2016). Nutrient supply controls picoplankton community structure during three contrasting seasons in the northwestern Mediterranean Sea. *Marine Ecology Progress Series*, *543*, 1–19. https://doi.org/10.3354/meps11558

Mouriño-Carballido, B., Otero Ferrer, J. L., Fernandez Castro, B., Maranon, E., Blazquez Maseda, M., Aguiar-Gonzalez, B., et al. (2021). Magnitude of nitrate turbulent diffusion in contrasting marine environments. *Scientific Reports*, *11*(1), 18804. https://doi.org/10.1038/s41598-021-97731-4

Otero-Ferrer, J. L., Cermeño, P., Bode, A., Fernández-Castro, B., Gasol, J. M., Morán, X. A. G., et al. (2018). Factors controlling the community structure of picoplankton in contrasting marine environments. *Biogeosciences*, *15*(20), 6199–6220. https://doi.org/10.5194/bg-15-6199-2018

Painter, S. (2017). AMT19 (JC039) CTD profiles (pressure, temperature, salinity, potential temperature, density, fluorescence, transmissance, downwelling PAR, dissolved oxygen concentration) calibrated and binned to 1 dbar [Dataset]. *British Oceanographic Data Centre - Natural Environment Research Council, UK*. https://doi.org/10.5285/2223243a-65b9-0f04-e053-6c86abc0ed45

Painter, S., Hopkins, J., & Allen, J. T. (2017). AMT18 (JR20081003) CTD profiles (pressure, temperature, salinity, potential temperature, density, fluorescence, transmissance, downwelling PAR, dissolved oxygen concentration) calibrated and binned to 1 dbar [Dataset]. *British Oceanographic Data Centre - Natural Environment Research Council, UK*. https://doi.org/10.5285/2223243a-65ba-0f04-e053-6c86abc0ed45

Painter, S. C., Patey, M. D., Forryan, A., & Torres-Valdes, S. (2013). Evaluating the balance between vertical diffusive nitrate supply and nitrogen fixation with reference to nitrate uptake in the eastern subtropical North Atlantic Ocean. *Journal of Geophysical Research: Oceans*, *118*(10), 5732–5749. https://doi.org/10.1002/jgrc.20416

Painter, S. C., Patey, M. D., Tarran, G. A., & Torres-Valdes, S. (2014). Picoeukaryote distribution in relation to nitrate uptake in the oceanic nitracline. *Aquatic Microbial Ecology*, *72*(3), 195–213. https://doi.org/10.3354/ame01695

Painter, S. C., Sanders, R., Poulton, A. J., Woodward, E. M. S., Lucas, M., & Chamberlain, K. (2007). Nitrate uptake at photic zone depths is not important for export in the subtropical ocean. *Global Biogeochemical Cycles*, *21*(4), GB4005. https://doi.org/10.1029/2006gb002807

Poulton, A. J., Holligan, P. M., Charalampopoulou, A., & Adey, T. R. (2017). Coccolithophore ecology in the tropical and subtropical Atlantic Ocean: New perspectives from the Atlantic Meridional Transect (AMT) programme. *Progress in Oceanography*, *158*, 150–170. https://doi.org/10.1016/j.pocean.2017.01.003

Probyn, T. A., Waldron, H. N., Searson, S., & Owens, N. J. P. (1996). Diel variability in nitrogenous nutrient uptake at photic and subphotic depths. *Journal of Plankton Research*, *18*(11), 2063–2079. https://doi.org/10.1093/plankt/18.11.2063

Rafter, P. A., Bagnell, A., Marconi, D., & DeVries, T. (2019). Global trends in marine nitrate N isotopes from observations and a neural network-based climatology. *Biogeosciences*, *16*(13), 2617–2633. https://doi.org/10.5194/bg-16-2617-2019

Ramsing, N. B., Fossing, H., Ferdelman, T. G., Andersen, F., & Thamdrup, B. (1996). Distribution of bacterial populations in a stratified fjord (Mariager fjord, Denmark) quantified by in situ hybridization and related to chemical gradients in the water column. *Applied and Environmental Microbiology*, *62*(4), 1391–1404. https://doi.org/10.1128/aem.62.10.3914-3914b.1996

Rees, A., Robinson, C., Smyth, T., Aiken, J., Nightingale, P., & Zubkov, M. (2015). 20 years of the Atlantic meridional Transect-AMT. *Limnology and Oceanography Bulletin*, *24*(4), 101–107. https://doi.org/10.1002/lob.10069

Rees, A. P., Smyth, T. J., & Brotas, V. (2024). Editorial: The Atlantic meridional transect programme (1995-2023). *Frontiers in Marine Science*, *11*, 1358174. https://doi.org/10.3389/fmars.2024.1358174

Rees, A. P., Woodward, E. M. S., & Joint, I. (2006). Concentrations and uptake of nitrate and ammonium in the Atlantic Ocean between 60°N and 50°S. *Deep-Sea Research Part II*, *53*(14–16), 1649–1665. https://doi.org/10.1016/j.dsr2.2006.05.008

Robinson, C., Holligan, P., Jickells, T., & Lavender, S. (2009). Foreward: The Atlantic meridional transect Programme (1995-2012). *Deep-Sea Research Part II*, *56*(15), 895–898. https://doi.org/10.1016/j.dsr2.2008.10.005

Robinson, C., Poulton, A. J., Holligan, P. M., Baker, A. R., Forster, G., Gist, N., et al. (2006). The Atlantic Meridional Transect (AMT) Programme: A contextual view 1995-2005. *Deep-Sea Research Part II*, *53*(14–16), 1485–1515. https://doi.org/10.1016/j.dsr2.2006.05.015

Shao, Z., Xu, Y., Wang, H., Luo, W., Wang, L., Huang, Y., et al. (2023). Global oceanic diazotroph database version 2 and elevated estimate of global oceanic N_2 fixation. *Earth System Science Data*, *15*(8), 3673–3709. https://doi.org/10.5194/essd-15-3673-2023

Silsbe, G. M., Fox, J., Westberry, T. K., & Halsey, K. H. (2025). Global declines in net primary production in the ocean color era. *Nature Communications*, *16*(1), 5821. https://doi.org/10.1038/s41467-025-60906-y

Tarran, G. A. (2020a). Abundance of microbial bacteria and phytoplankton through the water column during the AMT26 (JR16001) cruise in September-November 2016 [Dataset]. *British Oceanographic Data Centre, National Oceanography Centre, NERC, UK*. https://doi.org/10.5285/a1c190c6-cfc8-4c68-e053-6c86abc0c633

Tarran, G. A. (2020b). Abundance of microbial bacteria and phytoplankton through the water column during the AMT29 (DY110) cruise in October-November 2019 [Dataset]. *British Oceanographic Data Centre, National Oceanography Centre, NERC, UK*. https://doi.org/10.5285/a147c314-688a-55e9-e053-6c86abc0dc81

Tarran, G. A., Heywood, J. L., & Zubkov, M. V. (2006). Latitudinal changes in the standing stocks of nano- and picoeukaryotic phytoplankton in the Atlantic Ocean. *Deep-Sea Research Part II*, *53*(14–16), 1516–1529. https://doi.org/10.1016/j.dsr2.2006.05.004

Tarran, G. A., Lange, P. K., & Zubkov, M. V. (2020). Abundance of microbial phytoplankton through the water column during the AMT25 (JR15001) cruise in September-November 2015 [Dataset]. *British Oceanographic Data Centre, National Oceanography Centre, NERC, UK*. https://doi.org/10.5285/a2104adc-e98e-6789-e053-6c86abc0d557

Tarran, G. A., & May, R. (2020a). Abundance of microbial bacteria and phytoplankton through the water column during the AMT27 (DY084/DY085) cruise in September-November 2017 [Dataset]. *British Oceanographic Data Centre, National Oceanography Centre, NERC, UK*. https://doi.org/10.5285/a147c314-688c-55e9-e053-6c86abc0dc81

Tarran, G. A., & May, R. (2020b). Abundance of microbial bacteria and phytoplankton through the water column during the AMT28 (JR18001) cruise in September-October 2018 [Dataset]. *British Oceanographic Data Centre, National Oceanography Centre, NERC, UK*. https://doi.org/10.5285/a147c314-688b-55e9-e053-6c86abc0dc81

Tarran, G. A., & Zubkov, M. V. (2020a). Abundance of microbial bacteria and phytoplankton through the water column during the AMT13 (JR20030910/JR91) cruise in September-October 2003 [Dataset]. *British Oceanographic Data Centre, National Oceanography Centre, NERC, UK*. https://doi.org/10.5285/a2104adc-e997-6789-e053-6c86abc0d557

Tarran, G. A., & Zubkov, M. V. (2020b). Abundance of microbial bacteria and phytoplankton through the water column during the AMT16 (D294) cruise in May-June 2005 [Dataset]. *British Oceanographic Data Centre, National Oceanography Centre, NERC, UK*. https://doi.org/10.5285/a2104adc-e996-6789-e053-6c86abc0d557

Tarran, G. A., & Zubkov, M. V. (2020c). Abundance of microbial phytoplankton through the water column during the AMT18 (JR20081003/JR218) cruise in October-November 2008 [Dataset]. *British Oceanographic Data Centre, National Oceanography Centre, NERC, UK*. https://doi.org/10.5285/a2104adc-e995-6789-e053-6c86abc0d557

Tarran, G. A., & Zubkov, M. V. (2020d). Abundance of microbial phytoplankton through the water column during the AMT19 (JC039) cruise in October-December 2009 [Dataset]. *British Oceanographic Data Centre, National Oceanography Centre, NERC, UK*. https://doi.org/10.5285/a2104adc-e994-6789-e053-6c86abc0d557

Tarran, G. A., & Zubkov, M. V. (2020e). Abundance of microbial phytoplankton through the water column during the AMT20 (JC053) cruise in October-November 2010 [Dataset]. *British Oceanographic Data Centre, National Oceanography Centre, NERC, UK*. https://doi.org/10.5285/a2104adc-e993-6789-e053-6c86abc0d557

Tarran, G. A., & Zubkov, M. V. (2020f). Abundance of microbial phytoplankton through the water column during the AMT21 (D371) cruise in September-November 2011 [Dataset]. *British Oceanographic Data Centre, National Oceanography Centre, NERC, UK*. https://doi.org/10.5285/a2104adc-e992-6789-e053-6c86abc0d557

Tarran, G. A., & Zubkov, M. V. (2020g). Abundance of microbial phytoplankton through the water column during the AMT22 (JC079) cruise in October-November 2012 [Dataset]. *British Oceanographic Data Centre, National Oceanography Centre, NERC, UK*. https://doi.org/10.5285/a2104adc-e991-6789-e053-6c86abc0d557

Tarran, G. A., & Zubkov, M. V. (2020h). Abundance of microbial phytoplankton through the water column during the AMT23 (JR20131005/JR300) cruise in October-November 2013 [Dataset]. *British Oceanographic Data Centre, National Oceanography Centre, NERC, UK*. https://doi.org/10.5285/a2104adc-e990-6789-e053-6c86abc0d557

Tarran, G. A., & Zubkov, M. V. (2020i). Abundance of microbial phytoplankton through the water column during the AMT24 (JR20140922/JR303) cruise in September-November 2014 [Dataset]. *British Oceanographic Data Centre, National Oceanography Centre, NERC, UK*. https://doi.org/10.5285/a2104adc-e98f-6789-e053-6c86abc0d557

Thomas, R. W. (2016). AMT21 (D371) CTD profiles (pressure, temperature, salinity, potential temperature, density, fluorescence, transmissance, downwelling PAR, dissolved oxygen concentration) calibrated and binned to 1 dbar [Dataset]. *British Oceanographic Data Centre - Natural Environment Research Council, UK*. https://doi.org/10.5285/2223243a-65b8-0f04-e053-6c86abc0ed45

Thomas, R. W. (2017a). AMT20 (JC053) CTD profiles (pressure, temperature, salinity, potential temperature, density, fluorescence, transmissance, downwelling PAR, dissolved oxygen concentration) calibrated and binned to 1 dbar [Dataset]. *British Oceanographic Data Centre - Natural Environment Research Council, UK*. https://doi.org/10.5285/2223243a-65b7-0f04-e053-6c86abc0ed45

Thomas, R. W. (2017b). AMT22 (JC079) CTD profiles (pressure, temperature, salinity, potential temperature, density, fluorescence, transmissance, downwelling PAR, dissolved oxygen concentration) calibrated and binned to 1 dbar [Dataset]. *British Oceanographic Data Centre - Natural Environment Research Council, UK*. https://doi.org/10.5285/4b64e646-89d0-3b66-e053-6c86abc0e62f

Thomas, R. W. (2021). JR20140922 (AMT24, JR303) CTD profiles (pressure, temperature, salinity, potential temperature, density, fluorescence, transmissance, downwelling PAR, dissolved oxygen concentration) calibrated and binned to 1 dbar [Dataset]. *NERC EDS British Oceanographic Data Centre NOC*. https://doi.org/10.5285/c0152486-cdae-4744-e053-6c86abc050c2

Thorpe, S. A. (2005). *The turbulent Ocean*. Cambridge University Press.

Villamaña, M., Marañón, E., Cermeño, P., Estrada, M., Fernández-Castro, B., Figueiras, F. G., et al. (2019). The role of mixing in controlling resource availability and phytoplankton community composition. *Progress in Oceanography*, *178*, 102181. https://doi.org/10.1016/j.pocean.2019.102181

Waterhouse, A. F., MacKinnon, J. A., Nash, J. D., Alford, M. H., Kunze, E., Simmons, H. L., et al. (2014). Global patterns of diapycnal mixing from measurements of the turbulent dissipation rate. *Journal of Physical Oceanography*, *44*(7), 1854–1872. https://doi.org/10.1175/jpo-d-13-0104.1

Woodward, E. M. S., & Beesley, A. (2022). Atlantic Meridional Transect cruise AMT21 (D371) micro-molar nutrient measurements from CTD bottle samples collected in 2011 [Dataset]. *NERC EDS British Oceanographic Data Centre NOC*. https://doi.org/10.5285/c73b01f0-c016-4312-e053-6c86abc08369

Woodward, E. M. S., & Harris, C. (2015). AMT23 (JR20131005) micro-molar nutrient measurements from CTD bottle samples [Dataset]. *British Oceanographic Data Centre - Natural Environment Research Council, UK*. https://doi.org/10.5285/215a1e9b-428c-52f5-e053-6c86abc06d17

Woodward, E. M. S., & Harris, C. (2019a). Atlantic Meridional Transect cruise AMT26 (JR16001) micro-molar nutrient measurements from CTD bottle samples collected in 2016 [Dataset]. *British Oceanographic Data Centre, National Oceanography Centre, NERC, UK*. https://doi.org/10.5285/82692b93-3bec-26da-e053-6c86abc00e14

Woodward, E. M. S., & Harris, C. (2019b). Atlantic Meridional Transect cruise AMT27 (DY084) micro-molar nutrient measurements from CTD bottle samples during 2017 [Dataset]. *British Oceanographic Data Centre, National Oceanography Centre, NERC, UK*. https://doi.org/10.5285/915141ee-46c9-4da1-e053-6c86abc09800

Woodward, E. M. S., & Harris, C. (2022c). Atlantic Meridional Transect cruise AMT18 (JR20081003/JR218) micro-molar nutrient measurements from CTD bottle samples collected in 2008 [Dataset]. *NERC EDS British Oceanographic Data Centre NOC*. https://doi.org/10.5285/c73b01f0-c015-4312-e053-6c86abc08369

Woodward, E. M. S., & Harris, C. (2022a). Atlantic Meridional Transect cruise AMT22 (JC079) micro-molar nutrient measurements from CTD bottle samples collected in 2012 [Dataset]. *NERC EDS British Oceanographic Data Centre NOC*. https://doi.org/10.5285/c73b01f0-c017-4312-e053-6c86abc08369

Woodward, E. M. S., & Harris, C. (2022b). Atlantic Meridional Transect cruise AMT24 (JR20140922/JR303) micro-molar nutrient measurements from CTD bottle samples collected in 2014 [Dataset]. *NERC EDS British Oceanographic Data Centre NOC*. https://doi.org/10.5285/c73b01f0-c018-4312-e053-6c86abc08369

Woodward, E. M. S., Harris, C., & May, R. (2021). Atlantic Meridional Transect cruise AMT29 (DY110) in 2019, micro-molar nutrient measurements from CTD bottle samples [Dataset]. *British Oceanographic Data Centre, National Oceanography Centre, NERC, UK*. https://doi.org/10.5285/b6a76b41-a606-47b9-e053-6c86abc0c78f

Woodward, E. M. S., Harris, C., & Tuerena, R. (2018). AMT25 (JR15001) micro-molar nutrient measurements from CTD bottle samples [Dataset]. *British Oceanographic Data Centre - Natural Environment Research Council, UK*. https://doi.org/10.5285/7c1ca6b7-90c1-0e11-e053-6c86abc0077e

Woodward, E. M. S., & Rees, A. P. (2001). Nutrient distributions in an anticyclonic eddy in the northeast Atlantic Ocean, with reference to nanomolar ammonium concentrations. *Deep Sea Research Part II: Topical Studies in Oceanography*, *48*(4–5), 775–793. https://doi.org/10.1016/s0967-0645(00)00097-7

Worden, A. Z., & Not, F. (2008). Ecology and diversity of picoeukaryotes. In D. L. Kirchman (Ed.), *Microbial ecology of the Oceans* (2nd ed., pp. 159–205). John Wiley and Sons, Inc.

Xing, X., Xiu, P., Laws, E. A., Yang, G., Liu, X., & Chai, F. (2023). Light-Driven and nutrient-driven displacements of subsurface chlorophyll maximum depth in subtropical gyres. *Geophysical Research Letters*, *50*(22), e2023GL104510. https://doi.org/10.1029/2023gl104510

Yool, A., Martin, A. P., Fernandez, C., & Clark, D. R. (2007). The significance of nitrification for oceanic new production. *Nature*, *447*(7147), 999–1002. https://doi.org/10.1038/nature05885

Zehr, J. P., & Capone, D. G. (2021). *Marine nitrogen fixation* (p. 186). Springer Nature.

Zubkov, M. V., Sleigh, M. A., & Burkill, P. H. (2000). Assaying picoplankton distribution by flow cytometry or underway samples collected along a meriodional transect across the Atlantic Ocean. *Aquatic Microbial Ecology*, *21*, 13–20. https://doi.org/10.3354/ame021013

Zubkov, M. V., Sleigh, M. A., Burkill, P. H., & Leakey, R. J. G. (2000). Picoplankton community structure on the Atlantic Meridional Transect: A comparison between seasons. *Progress in Oceanography*, *45*(3–4), 369–386. https://doi.org/10.1016/s0079-6611(00)00008-2

Zubkov, M. V., Sleigh, M. A., Tarran, G. A., Burkhill, P. H., & Leakey, R. J. G. (1998). Picoplankton community structure on an Atlantic transect from 50°N to 50°S. *Deep-Sea Research Part I*, *45*(8), 1339–1355. https://doi.org/10.1016/s0967-0637(98)00015-6